was collected, and the protein concentration was determined. The lysate (50 μg) was separated by SDS-polyacrylamide gel electrophoresis and transferred onto polyvinylidene difluoride membranes. After blocking the membrane, the blots were incubated with antisera against alpha-SMA or beta-actin (Sigma-Aldrich). The bound antibody was detected on X-ray film by enhanced chemiluminescence (ECL) with horseradish peroxidase-conjugated secondary antibodies and cyclic diacylhydrazides (GE Healthcare Bio-Sciences Corp., Piscataway, NJ, USA). The levels of beta-actin were examined as internal control.

Real-time RCR in embryonic and neonatal kidney

In the case of embryonic and neonatal kidney, Wistar/ST rats at various stages of gestation were purchased from Shimizu Laboratory Supplies Co., Ltd. (Kyoto, Japan); the kidneys were then collected from 9 to 12 embryos of the same maternal rat. We used three separate batches of maternal rats.

References

1. **Kawachi H, Koike H, Kurihara H, Sakai T, Shimizu F.** Cloning of rat homologue of podocin: Expression in proteinuric states and in developing glomeruli. *J Am Soc Nephrol* 13: 46-56, 2003.
2. **Nishimura M, Kakigi A, Takeda T, Takeda S, Doi K.** Expression of aquaporins, vasopressin type 2 receptor, and Na^+-K^+-Cl^- cotransporters in the rat endolymphatic sac. *Acta Oto-Laryngologica* 129: 812-818, 2009.
3. **Takahashi K, Masuda S, Nakamura N, Saito H, Futami T, Doi T, Inui K.** Upregulations of H^+-peptide cotoransporter PEPT2 in rat remant kidney. *Am J*

Physiol Renal Physiol 281: F1109-1116, 2001.

Biochemical Pharmacology 79 (2010) 67–76

Contents lists available at ScienceDirect

Biochemical Pharmacology

journal homepage: www.elsevier.com/locate/biochempharm

mTOR inhibitor everolimus ameliorates progressive tubular dysfunction in chronic renal failure rats

Shunsaku Nakagawa, Satohiro Masuda, Kumiko Nishihara, Ken-ichi Inui *

Department of Pharmacy, Kyoto University Hospital, Faculty of Medicine, Kyoto University, Sakyo-ku, Kyoto 606-8507, Japan

ARTICLE INFO

Article history:
Received 16 June 2009
Accepted 28 July 2009

Keywords:
Mammalian target of rapamycin
Proximal tubule injury
Albuminuria
Drug transporter
Chronic kidney disease

ABSTRACT

Responsible factors in progressive tubular dysfunction in chronic renal failure have not been fully identified. In the present study, we hypothesized that the mammalian target of rapamycin, mTOR, was a key molecule in the degenerative and progressive tubular damage in chronic renal failure. Everolimus, an mTOR inhibitor, was administered for 14 days in 5/6 nephrectomized (Nx) rats at 2 and 8 weeks after renal ablation. Marked activation of the mTOR pathway was found at glomeruli and proximal tubules in remnant kidneys of Nx rats. The reduced expression levels of the phosphorylated S6 indicated the satisfactory pharmacological effects of treatment with everolimus for 14 days. Everolimus suppressed the accumulation of smooth muscle alpha actin, infiltration of macrophages and expression of kidney injury molecule-1 in the proximal tubules. In addition, everolimus-treatment restored the tubular reabsorption of albumin, and had a restorative effect on the expression levels of membrane transporters in the polarized proximal tubular epithelium, when its administration was started at 8 weeks after Nx. These results indicate that the constitutively activated mTOR pathway in proximal tubules has an important role in the progressive tubular dysfunction, and that mTOR inhibitors have renoprotective effects to improve the proximal tubular functions in end-stage renal disease.

1. Introduction

In chronic renal failure (CRF), the irreversible and progressive loss of nephrons ultimately results in glomerular sclerosis, tubular atrophy and further reductions in nephron numbers [1,2]. These physiological changes produce a complex series of adverse effects that eventuate in progressive renal injury and a severe decline in function. We have demonstrated expressional and functional alterations of drug transporters in the proximal tubules of 5/6 nephrectomized (Nx) rats, a model of CRF [3–6]. Furthermore, levels of tubular transporters that play important roles in the handling of nutrients and electrolytes were also decreased in Nx rats [7,8]. Therefore, a decline in tubular functions causes the accumulation of uremic toxin, metabolites and xenobiotics and increases renal dysfunction and systemic toxicity [9,10]. Consequently, it is important to understand the molecular mechanisms behind in CRF and improve therapeutic approaches for the progressive tubular dysfunction.

Mammalian target of rapamycin, mTOR, is a serine/threonine kinase that regulates a variety of cellular processes including growth, proliferation and metabolism [11–13]. mTOR inhibitors such as rapamycin (sirolimus) and everolimus are generally used as immunosuppressants to prevent immunological reactions after organ transplantation. Everolimus is an immunosuppressive macrolide derived from rapamycin. Although they exhibit slightly different pharmacokinetic properties, both everolimus and rapamycin exert their effects by the same mechanism [12]. Each drug binds to the intracellular cofactor FK506-binding protein (FKBP12) to form a complex, which then binds to mTOR interfering signal transduction to its downstream effectors.

Recently, it was reported that rapamycin reduced interstitial fibrosis and glomerular sclerosis after kidney transplantation in patients with chronic allograft nephropathy [14,15]. In addition, a causal link between the activation of the mTOR pathway and the progression of polycystic kidney disease or diabetic nephropathy was reported [16–18]. However, it is still unclear whether the mTOR pathway associates with tubular functions such as the reabsorption of nutrients and secretion of xenobiotics and metabolites.

Previous studies suggest the relationship between the mTOR pathway and the progression of CRF. Diekmann et al. [19] reported that rapamycin abolished the progression of proteinuria and structural damage when administered from the 6th week after nephrectomy in CRF rats, while Vogelbacher et al. [20] reported that everolimus induced renal deterioration and proteinuria when given from the 3rd day after nephrectomy. These findings encouraged us to examine the pharmacological effects of everolimus in Nx rats,

* Corresponding author. Tel.: +81 75 751 3577; fax: +81 75 751 4207.
E-mail address: inui@kuhp.kyoto-u.ac.jp (K.-i. Inui).

0006-2952/$ – see front matter © 2009 Elsevier Inc. All rights reserved.
doi:10.1016/j.bcp.2009.07.015

focusing on tubular functions, by subcutaneously administration of everolimus at 2 and 8 weeks after renal ablation. Our findings revealed the constitutive activation of the mTOR pathway at proximal tubules in the remnant kidneys, and the therapeutic effects of everolimus for the progression of tubular dysfunction in CRF.

2. Materials and methods

2.1. Animals

The experimental design is shown in Fig. 1. For ablation of the renal mass, male Wistar/ST rats (180–200 g) were anesthetized with sodium pentobarbital (50 mg/kg) and the kidneys were exposed under aseptic conditions via a ventral abdominal incision. The right kidney was removed, the posterior and anterior apical segmental branches of the left renal artery were individually ligated, and the abdominal incision was closed with 4-0 silk sutures [3,4]. After surgery, animals were allowed to recover from anesthesia and surgery in cages with free access to water and standard rat chow. To investigate the effects of the mTOR inhibitor everolimus on the progression of CRF, rats were administered everolimus (LC Laboratories, Woburn, MA; 2 mg/kg body weight, E(+)) or vehicle (E(−)) subcutaneously for 14 days. The administration of everolimus was initiated at 2 and 8 weeks after surgery. After the 14-day administration, the subsequent experiments were carried out. The concentration of everolimus in whole blood samples was measured using LC/MS/MS [21]. The experiments with animals were performed in accordance with the *Guidelines for Animal Experiments of Kyoto University*. All protocols were previously approved by the Animal Research Committee, Graduate School of Medicine, Kyoto University.

2.2. Renal function and histology

Rats were maintained in metabolic cages for 24 h to collect 24-h urine samples. The animals were fed normal pellet food ad libitum, and given water freely in metabolic cages. Then, rats were anesthetized with an intraperitoneal administration of 50 mg/kg sodium pentobarbital to collect plasma and kidneys. Urinary albumin was assessed using an enzyme-linked immunosorbent assay (ELISA) kit (Nephrat II) (Exocell, Inc., Philadelphia, PA). The levels of creatinine in plasma and urine were determined with the Jaffé reaction. The BUN concentration was determined by the urease/indophenol method. For measurements, we used assay kits from Wako Pure Chemical Industries (Osaka, Japan). Kidneys were fixed in ethyl Carnoy's solution and stained with periodic acid-Schiff (PAS) reagent by Sapporo General Pathology Laboratory Co., Ltd. (Hokkaido, Japan). The glomerular diameter and inside diameter of tubules were determined as the mean value from 20 glomeruli and 40 proximal tubules, respectively.

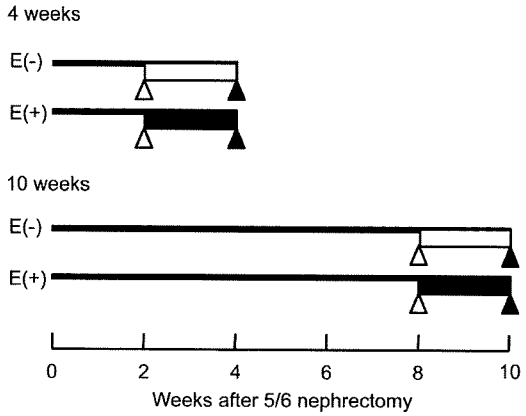

Fig. 1. Experimental design. Rats were administered everolimus (2 mg/kg body weight, E(+)) or vehicle E(−)) subcutaneously for 14 days. The trough concentration of everolimus at the 15th day was 18.4 ± 1.2 ng/mL. The administration of everolimus was initiated at 2 and 8 weeks after 5/6 nephrectomy. Open triangle, initiation of administration; closed triangle, sample collection; open bar, administration of vehicle; closed bar, administration of everolimus.

2.3. Western blot analysis

The rat whole kidney was homogenized in lysis buffer (50 mM Tris–HCl, pH 7.5, 150 mM NaCl, 10 mM NaF, 1 mM $Na_4P_2O_7$, 100 mM Na_3VO_4, 1% NP-40 and 1% protease inhibitor cocktail (Nacalai Tesque, Kyoto, Japan)). The tissue lysate was clarified by centrifugation, and protein concentrations were determined with the Bradford protein assay (Bio-Rad Laboratories, Hercules, CA). The crude membrane fractions of the rat kidney were prepared as described [22]. The kidney lysate was used for the analyze the protein levels of phosphorylated Akt (p-Akt), mTOR (p-mTOR), S6 kinase (p-S6 kinase), ribosomal protein S6 (p-S6), kidney injury molecule-1 (Kim-1), smooth muscle alpha actin (alpha-SMA), beta-actin and GAPDH. The membrane fraction was used for Na^+/D-glucose cotransporter (SGLT) 1, Na^+/H^+ exchanger (NHE) 3, H^+/peptide cotransporter (PEPT) 1, PEPT2, organic cation transporter (OCT) 1, OCT2 organic anion transporter (OAT) 1, OAT3, H^+/organic cation antiporter (MATE, multidrug and toxin extrusion) 1, P-glycoprotein (P-gp) and the Na^+/K^+-ATPase alpha1 subunit. Equal amount of the lysate or membrane fraction was separated by sodium dodecyl sulfate-polyacrylamide gel electrophoresis (SDS-PAGE) and transferred to polyvinylidene difluoride (PVDF) membranes (Millipore, Billerica, MA). The blots were blocked, washed, and incubated with the primary antibodies (for total Akt, p-Akt, total mTOR, p-mTOR, p-S6K, total S6, p-S6 (Cell Signaling Technology, Danvers, MA), GAPDH (Santa Cruz Biotechnology, Avenue, CA), alpha-SMA, beta-actin (Sigma), Kim-1 (generated in our laboratory referring to the report by Ichimura et al. [23], Fig. 2),

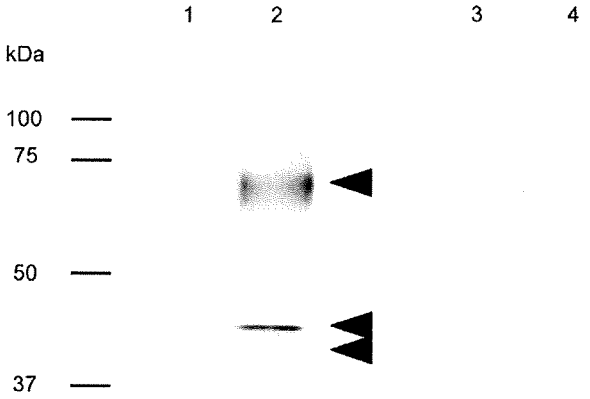

Fig. 2. Polyclonal antibody against Kim-1. Polyclonal antibody was raised against the synthetic peptide corresponding to the R9 region of rat Kim-1 (HPRAEDNIYIIEDRSRG) [23]. Tissue lysates (50 μg) from normal kidney (lanes 1 and 3) or Nx rat kidneys at 10 weeks after surgery (lanes 2 and 4) were separated by SDS-PAGE and blotted onto PVDF membranes. Antibody specific for Kim-1 (lanes 1 and 2) or antibody preabsorbed with the synthetic antigen peptide (10 μg/mL) (lanes 3 and 4) were used as primary antibody. Kim-1 protein was up-regulated in the Nx rat kidneys. The preabsorption of antibody with corresponding antigen peptide abolished these positive bands, showing the presence of Kim-1 protein in the rat kidney. Arrows indicate the position of the Kim-1 specific bands.

SGLT1, NHE3, Na^+/K^+-ATPase alpha1 subunit (Millipore), PEPT1 [24], PEPT2 [25], OCT1 [26], OCT2 [27], OAT1, OAT3 [4], MATE1 [6] and P-gp (monoclonal antibody C219 [28])) overnight at 4 °C. The bound antibody was detected on X-ray film by enhanced chemiluminescence (ECL) with horseradish peroxidase-conjugated secondary antibodies and cyclic diacylhydrazides (GE Healthcare Bio-Sciences Corp., Piscataway, NJ). Beta-actin, GAPDH and the Na^+/K^+-ATPase alpha1 subunit were examined as controls. The relative densities of the bands in each lane were determined using NIH Image J 1.39 (National Institute of Health, Bethesda, MD, USA).

2.4. Immunofluorescence analysis

Rats at 15th days after the daily administration of everolimus or vehicle from 2 or 8 weeks after surgery were used. After perfusion with 4% paraformaldehyde in PBS (Wako), and the kidneys were embedded in Tissue-Tek® O.C.T. compound (Sakura Finetechnical, Tokyo, Japan) and frozen rapidly in liquid nitrogen. Sections (6 μm thick) were cut and covered with 5% BSA in PBS containing 0.3% Triton X-100. The covered sections were incubated for overnight at 4 °C with the primary antibodies (1:200 dilution) specific for p-mTOR, p-S6, alpha-SMA, ED1 and rat Kim-1 (R&D Systems, Minneapolis, MN), washing three times, and incubated with secondary antibodies (Cy3-labeled donkey anti-rabbit IgG (ALTAG Laboratory, San Francisco, CA) for p-mTOR and p-S6, Alexa 546-labeled donkey anti-goat IgG (Invitrogen Japan K.K., Tokyo, Japan) for rat Kim-1, Alexa 546-labeled goat anti-mouse IgG (Invitrogen) for ED1 and alpha-SMA), Alexa 488-Phalloidin (Invitrogen), and DAPI (Wako, Osaka, Japan) at 37 °C for 60 min. These sections were examined under a fluorescence microscope BZ-9000 (KEYENCE, Osaka, Japan). Signals for secondary antibodies, Alexa 488-Phalloidin and DAPI were captured, and the images of each color signals in the same section were merged.

2.5. Infusion experiment

Renal distribution of fluorescein isothiocyanate-conjugated human albumin (FITC-albumin; Sigma, Deisenhofen, Germany) was measured in rats at 15th days after the daily administration of everolimus or vehicle from 8 weeks after surgery. Rats were anesthetized with an intraperitoneal administration of 50 mg/kg sodium pentobarbital, and catheterized at right femoral vein for the administration of FITC-albumin. Urine was collected from the urinary bladder catheterized with the tubing (Intramedic PE-50, Becton Dickinson and Co., Parsippany, NJ). Thereafter, FITC-albumin (5 mg/kg) was administered as a bolus via the femoral vein. Urine samples were collected during a 20-min period, and then, the kidneys were harvested. The FITC-albumin concentrations in urine were determined with an ELISA kit (AssayMax Human Albumin ELISA Kit) (ASSAYPRO, Triad South Drive St. Charles, MO). Fixed kidneys were frozen rapidly in liquid nitrogen. Sections (6 μm thick) were cut and incubated with Alexa 594-Phalloidin (Invitrogen) at 37 °C for 30 min. Signals for FITC-albumin or Alexa 594-Phalloidin were captured with a BZ-9000. Area of signals for FITC-albumin was calculated in three independent fields of renal cortex from six independent rats. The images of FITC-albumin and Alexa 594-Phalloidin in the same section were merged.

2.6. Statistical analysis

Data are expressed as means ± SEM. Data were statistically analyzed using the unpaired Student's *t*-test or multiple comparisons with Bonferroni's two-tailed test after a one-way ANOVA. Probability values of less than 0.05 were considered statistically significant. Statistical analysis was performed using Prism Version 4.0 software (GraphPad, San Diego, CA).

3. Results

3.1. Protein expression of phosphorylated Akt, mTOR, S6 kinase and S6

The phosphatidylinositol 3-kinases (PI3K)/Akt pathway is an upstream regulator of mTOR, and the activation of mTOR leads to the phosphorylation of downstream targets, such as S6 kinase and S6 [11,12]. After the 14 days' subcutaneous administration of everolimus (Fig. 1), the protein levels of p-Akt, p-mTOR, p-S6 kinase, p-S6 in the Nx rat kidneys were examined (Fig. 3). Although slight variations in the levels of total Akt, mTOR and S6 were observed, the levels of p-Akt, p-S6 kinase and p-S6 as well as p-mTOR were markedly increased in Nx rat kidneys compared to the control rat kidney (Fig. 3, Control vs. 4 weeks E(−) or 10 weeks E(−)). The treatment with everolimus markedly decreased the levels of p-S6 kinase and p-S6 (Fig. 3, 4 weeks E(−) vs. E(+), 10 weeks E(−) vs. E(+)). In addition, the levels of p-Akt and p-mTOR tended to decrease on treatment with everolimus, when the administration was started at 8 weeks after surgery (Fig. 3, 10 weeks E(−) vs. E(+)).

An immunofluorescence analysis revealed extensive staining of p-mTOR and p-S6 in the renal cortex (Fig. 4A–F). In the control rat kidneys, the signals for p-mTOR were predominantly observed in distal tubules (Fig. 4A, arrowhead), while the signals for p-S6 were observed in proximal tubules (Fig. 4B, arrow) as well as distal tubules (Fig. 4B, arrowhead). In the remnant kidneys, the staining

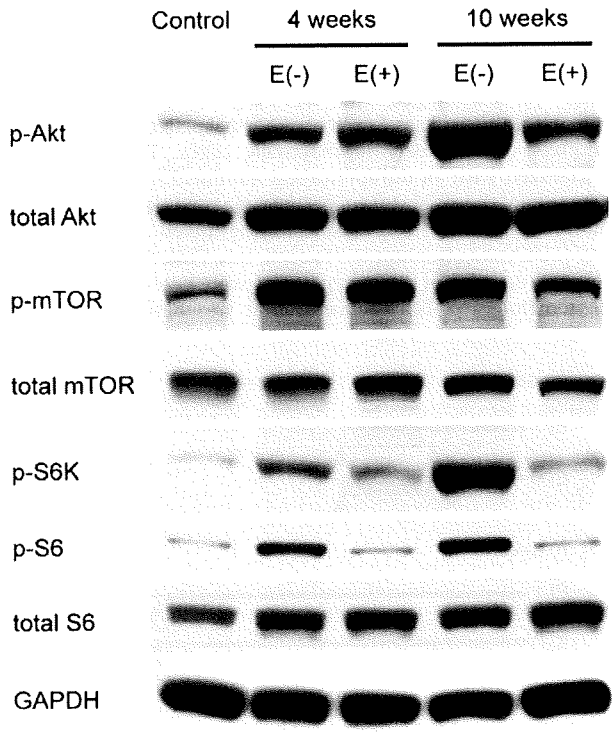

Fig. 3. Activation of the mTOR pathway in Nx rat kidneys. Four weeks and 10 weeks represent groups in which a 14-day subcutaneous administration of everolimus (2 mg/kg/day) or vehicle was initiated at 2 and 8 weeks after surgery, respectively. Tissue lysate (50 μg) from total kidney was separated by SDS-PAGE and blotted onto PVDF membranes. Antisera specific for total Akt, p-Akt, total mTOR, p-mTOR, p-S6 kinase total S6, p-S6 and GAPDH (1:1000–4000 dilution) were used as primary antibody. Control, lysate obtained from normal kidney; E(−), Nx rats administered vehicle; E(+), Nx rats administered everolimus.

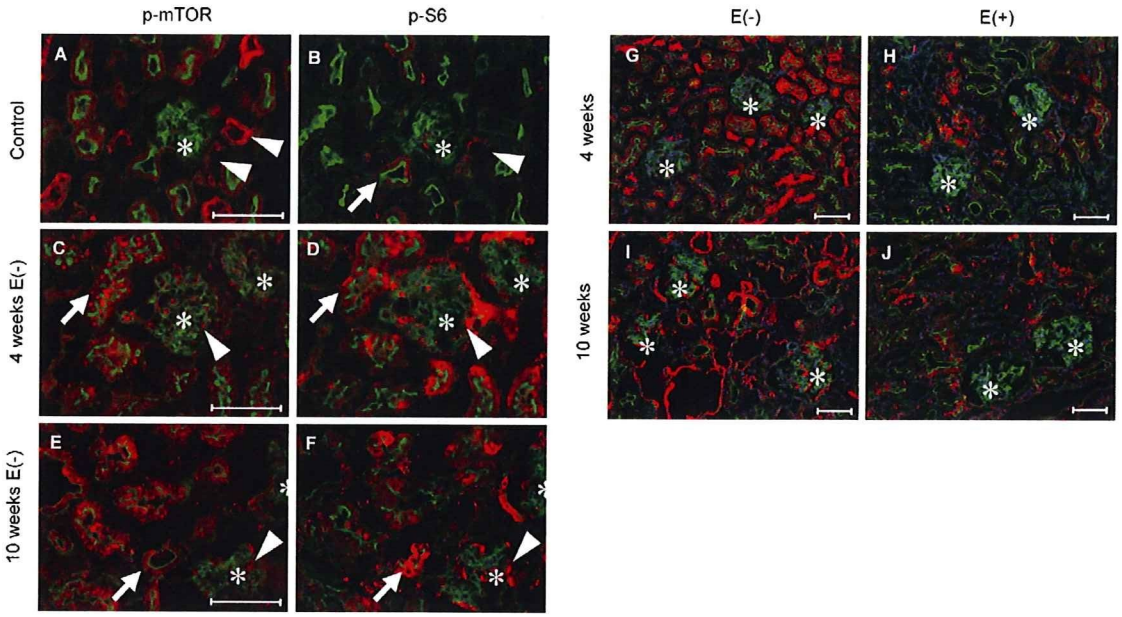

Fig. 4. Immunofluorescence analysis for p-mTOR and p-S6. (A–F) Serial sections of Nx rat kidneys are shown. Red signals for p-mTOR (A, C and E) or p-S6 (B, D and F) were merged with green signals for F-actin. (G–J) Effects of everolimus on the expression levels of p-S6 in Nx rats. Red signals for p-S6 were merged with green signals for F-actin and blue signals for DAPI. Symbols (*) represent the localization of glomeruli. Each scale bar represent a length of 100 μm. E(−), Nx rats administered vehicle; E(+), Nx rats administered everolimus.

of p-mTOR and p-S6 was intensified and aggregated in glomeruli (Fig. 4C–F, arrowheads) and the proximal tubular epithelial cells (Fig. 4C–F arrows). However, treatment with everolimus markedly decreased the intensity and area of signals for p-S6 (Fig. 4G–J).

3.2. Effects of everolimus on renal functions in Nx rats

As summarized in Table 1, significant changes in the kidney/body weight ratio, the urinary excretion of albumin (Ualb), and creatinine clearance (Ccr) and an increase in the level of blood urea nitrogen (BUN) were observed with time after renal ablation. When everolimus was administered daily for 14 days beginning at 2 weeks after surgery, significant decreases in Ccr and body weight were observed (Table 1, 4 weeks E(−) vs. E(+)). Although statistically not significant, the level of BUN tended to be increased by the administration of everolimus (Table 1, 4 weeks E(−) vs. E(+)). The kidney/body weight ratio and urinary excretion of albumin were markedly decreased when the administration of everolimus was initiated at 8 weeks after surgery, but the Ccr, level of BUN, body weight and urine volume were not affected by the administration of everolimus (Table 1, 10 weeks E(−) vs. E(+)).

3.3. Renal histology

Fig. 5A–D shows paraffin-embedded sections stained with PAS reagent. The glomerular diameter and inside diameter of tubules increased with time after the surgery (Fig. 5E and F, 4 weeks E(−) vs. 10 weeks E(−)). Glomerular hypertrophy and loss of the brush-border also progressed with time after renal ablation. However, these parameters were significantly decreased by the treatment with everolimus (Fig. 5E and F, 4weeks E(−) vs. E(+), 10 weeks E(−) vs. E(+)).

Strong signals for alpha-SMA and ED1 in the glomeruli (Fig. 6A, C, E and G; arrows) and tubulointerstitial space (Fig. 6A, C, E and G; arrowheads) were observed following Nx. However, the intensity of signals for alpha-SMA and the number of signals for ED1 decreased after the administration of everolimus (Fig. 6B, D, F and H). Furthermore, the expression levels of Kim-1 decreased after the administration of everolimus from 8 weeks after surgery (Fig. 6L), while proximal tubule-specific expression of Kim-1 increased with time after the surgery (Fig. 6I and K). Western blot analysis clearly showed that the expressional changes of alpha-SMA and Kim-1 were comparable with that observed in the immunofluorescence examination (Fig. 6M).

Table 1
Biochemical parameters in Nx rats.

	4 weeks		10 weeks	
	E(−)	E(+)	E(−)	E(+)
Body weight (g)	296 ± 15	242 ± 11*	361 ± 23	333 ± 18
Urine volume (mL/day)	33.1 ± 1.6	37.9 ± 3.5	31.8 ± 2.0	34.5 ± 4.5
Kidney weight/Body weight (%)	0.35 ± 0.03	0.27 ± 0.02	0.47 ± 0.04§	0.32 ± 0.01††
Ccr (mL/min/kg)	3.34 ± 0.51	1.61 ± 0.33*	1.32 ± 0.38§§	0.90 ± 0.29
BUN (mg/dL)	53.9 ± 8.7	111.4 ± 15.0	119.1 ± 31.3	120.7 ± 17.2
Ualb (mg/day)	46.5 ± 15.9	51.1 ± 16.3	128.7 ± 28.8§	45.6 ± 6.7†

Values are the mean ± SEM for six rats. Rats of 4 weeks and 10 weeks represent groups in which a 14-day subcutaneous administration of everolimus (2 mg/kg/day) or vehicle was initiated at 2 and 8 weeks after surgery, respectively. Ccr, creatinine clearance; BUN, blood urea nitrogen; Ualb, urinary albumin excretion; E(−), 5/6 nephrectomized rats administered vehicle; E(+), 5/6 nephrectomized rats administered everolimus. *$P < 0.05$, §$P < 0.05$, §§$P < 0.01$, significantly different from E(−) rats at 4 weeks. †$P < 0.05$, ††$P < 0.01$, significantly different from E(−) rats at 10 weeks.

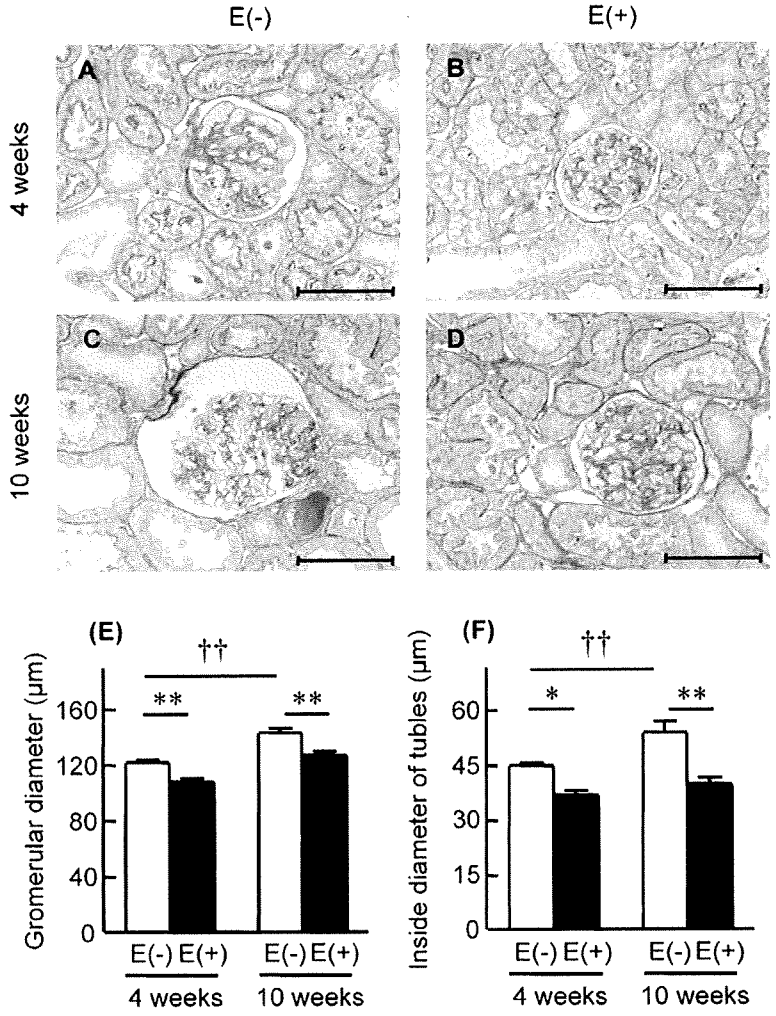

Fig. 5. Histological analysis of Nx rat kidneys. Four weeks and 10 weeks represent groups in which a 14-day subcutaneous injection was initiated at 2 and 8 weeks after surgery, respectively. (A–D) Representative photographs of PAS staining are shown. (E and F) Glomerular hypertrophy and tubular dilatation were assessed as described in the methods section. E(−), Nx rats administered vehicle; E(+), Nx rats administered everolimus. $^{\dagger\dagger}P < 0.01$, $^{*}P < 0.05$, $^{**}P < 0.01$, significantly different.

3.4. Reabsorption of FITC-albumin

Because everolimus significantly decreased the urinary excretion of albumin with minor changes in Ccr and the level of BUN (Table 1), the renal distribution of FITC-albumin was examined to visualize the restored reabsorptive function of proximal tubules (Fig. 7). The urinary FITC-albumin/creatinine ratio was significantly decreased to 31% in the Nx rats by treatment with everolimus from 8 weeks after renal ablation (Fig. 7E). Micrographs revealed green signals for FITC-albumin in the proximal tubules of the cortex where red signals for phalloidin were detected (Fig. 7A–D). In addition, the areas of green signals in the cortex were increased on the administration of everolimus (Fig. 7F), suggesting enhanced reabsorption of albumin from the filtered primary urine. In the kidneys of Nx rats administered vehicle, green signals were predominantly observed close to the brush-border membrane, with relatively weak signals detected at the side of the basolateral membrane (Fig. 7B). However, strong signals for albumin-containing vesicles were distributed throughout the proximal tubular epithelial cells in the everolimus-treated rat kidneys (Fig. 7D).

The treatment with everolimus decreased the number of proximal tubular epithelial cells positive for Kim-1 (Fig. 6), and then, we further analyzed the localization of Kim-1 in FITC-albumin administered rat kidneys (Fig. 7G and H). Immunofluorescence analysis with the antibody specific for Kim-1 showed that the injured proximal tubular epithelial cells, as indicated by red signals for Kim-1, contained little green signals for FITC-albumin (Fig. 7G and H). In contrast, tubular cells that contained strong signals for FITC-albumin were negative for Kim-1 (Fig. 7G and H).

3.5. Protein expression levels of transporters in proximal tubules

To obtain more information about the pharmacological effects of everolimus on tubular functions such as detoxicating systems and ion homeostasis, the protein levels of membrane transporters were examined (Fig. 8). Expression levels of 10 transporter proteins were depressed after surgery. Notably, the levels of NHE3, OCT1, OCT2, OAT1, OAT3, and MATE1 decreased with time after renal ablation. However, the levels of OCT1, OCT2, OAT1, OAT3 and MATE1 in the remnant kidneys after the administration of everolimus from 8 weeks after surgery were much higher than those in rats administered vehicle alone (Fig. 8, 10 weeks E(−) vs. E(+)), while everolimus tended to decrease the levels of OAT1, OAT3 and MATE1 when administered from 2 weeks after renal ablation (Fig. 8, 4 weeks E(−) vs. E(+)). In addition, the treatment with everolimus recovered the protein levels of NHE3 and PEPT2

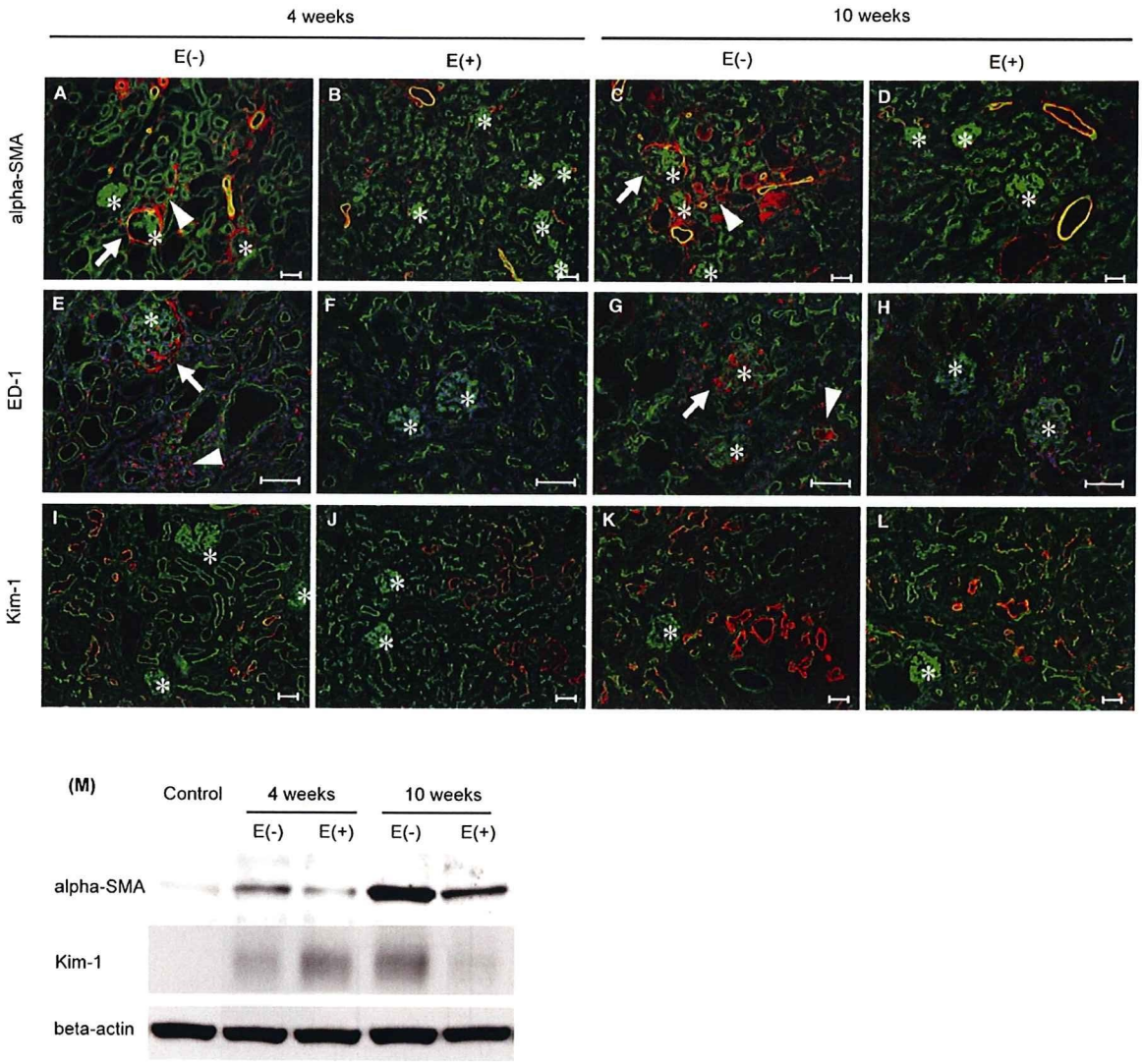

Fig. 6. Effects of the treatment with everolimus on the progression of CRF. Red signals for alpha-SMA (A-D), ED1 (E-H) and Kim-1 (I-L) in Nx rat kidneys were merged with green signals for F-actin and blue signals for DAPI. (M) Expression levels of alpha-SMA and Kim-1 were confirmed by Western blotting. Symbols (*) represent the localization of glomeruli. Scale bar: 100 μm. E(−), Nx rats administered vehicle; E(+), Nx rats administered everolimus.

independent on the timing of the initiation of treatment (Fig. 8, 4 weeks E(−) vs. E(+), 10 weeks E(−) vs. E(+)). In contrast, everolimus did not affect the levels of SGLT1, PEPT1 and P-gp. The effects of everolimus on the protein levels of membrane transporters, alpha-SMA and Kim-1 were summarized in Fig. 9.

4. Discussion

In the present study, we explored the role of mTOR pathway on the progression of CRF, and revealed the pathological significance of the mTOR pathway in the proximal tubular epithelium in CRF in vivo. Recently, the mTOR pathway has attracted attention for its roles in renal disease. It has been reported to regulate mesangial hypertrophy in diabetic nephropathy [17,18] and cyst formation in polycystic kidney disease [16,29], and to have an important role on the development of compensatory renal hypertrophy after nephron loss [30]. However, the role of the mTOR pathway in the proximal tubules was previously examined only in vitro such as using primary cultured mouse tubular cells [31] and the cultured human proximal tubule cell line, HK2 [32]. There have been no studies on its role in the progressive tubular dysfunction in CRF in vivo. In the present study, we found that the phosphrylation of Akt, mTOR, S6 kinase and S6 was enhanced in Nx rat kidneys at 4 and 10 weeks after surgery (Fig. 3), and the expression levels of p-mTOR and p-S6 were increased in glomeruli and proximal tubules (Fig. 4). In addition, the daily administration of everolimus for 14 days inhibited the activation of the mTOR pathway as indicated by the levels of p-S6 kinase and p-S6 in association with the signals for p-S6 in the proximal tubules as well as glomeruli (Figs. 3 and 4G–J). Furthermore, the treatment improved the urinary excretion of albumin and renal histology (Table 1, Figs. 5 and 7). These results indicated that the constitutively activated mTOR pathway in proximal tubules plays important roles in the progressive tubular dysfunction as well as glomerular lesions.

The aberrant albuminuria was considered to be due to the decreased reabsorption of albumin at proximal tubules as well as the increased permeability of the glomerular capillary wall [33]. Recently, it was reported that impaired tubular reabsorption of urinary albumin precedes the changes in glomerular permeability of macromolecules in early diabetic nephropathy [34]. In the

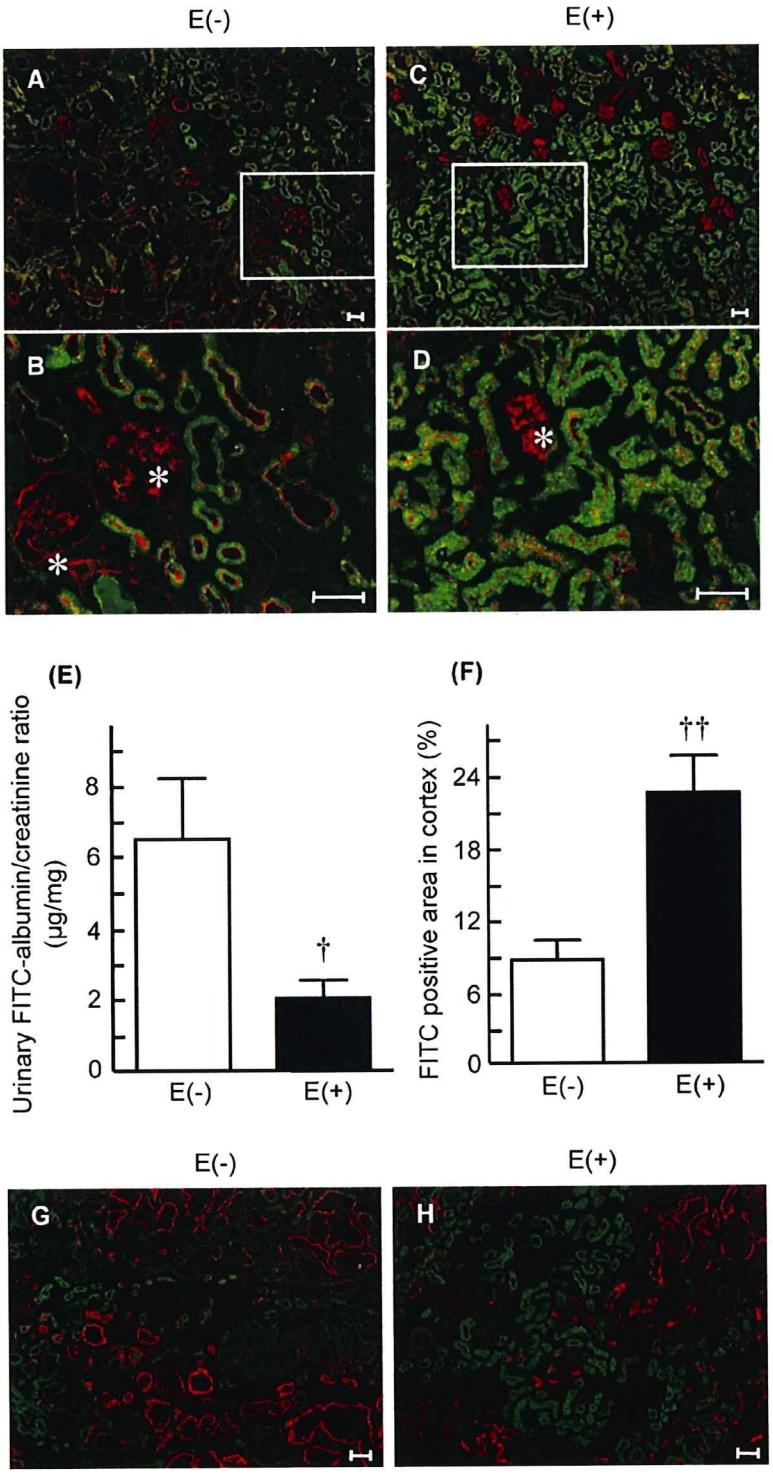

Fig. 7. Renal distribution of FITC-albumin. Nx rats 8 weeks after surgery were administered vehicle (E(−); A and B) or everolimus (2 mg/kg/day) (E(+); C and D) for 14 days. FITC-albumin (5 mg/kg) was administered as a bolus via the femoral vein. FITC (green) and F-actin (red) signals were merged in the same section. Urinary concentrations of FITC-albumin (E) and area of signals for FITC in renal cortex (F) were measured. $^{\dagger}P < 0.05$, $^{\dagger\dagger}P < 0.01$, significantly different. FITC (green) signals were merged in the same section with Kim-1 (red) signals (G and H). Scale bar: 100 μm. Symbols (*) represent the localization of glomeruli.

present study, the treatment with everolimus inhibited the progression of albuminuria (Table 1), and this phenomenon was in part due to the increase in its reabsorption at the proximal tubules (Fig. 7A–D and F) rather than the decreased permeability of the glomerular capillary wall without a marked response in glomerular function to everolimus-treatment (Table 1). On the other hand, it was reported that mTOR inhibition impaired the podocyte's integrity essential as a glomerular filtration barrier for albumin [35]. These findings and backgrounds suggest that everolimus-treatment restores the reabsorbing activity of albumin

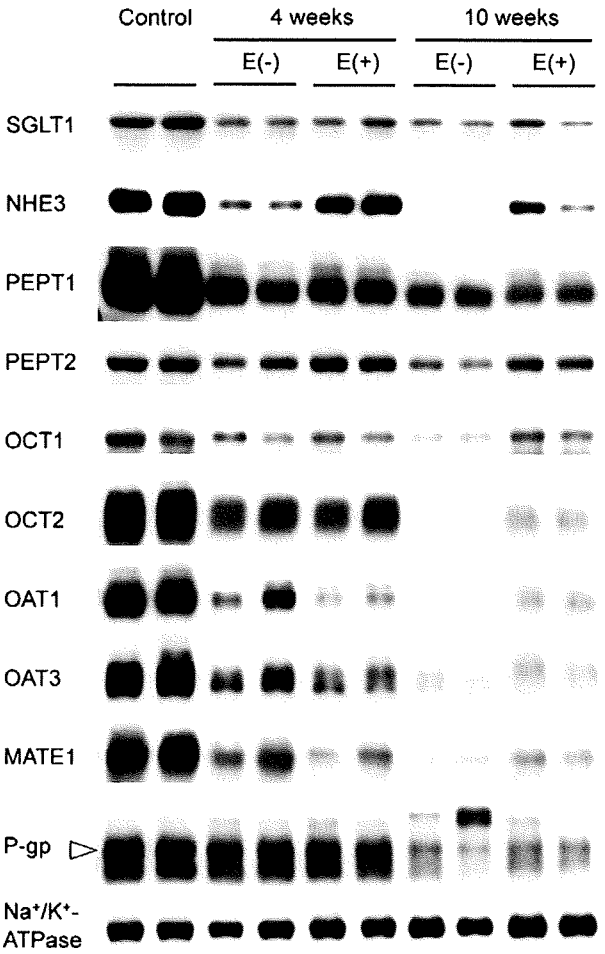

Fig. 8. Expression of proximal tubular transporters in the crude plasma membrane fractions of remnant kidneys. Four weeks and 10 weeks represent groups in which a 14-day subcutaneous administration of everolimus (2 mg/kg/day) or vehicle was initiated at 2 and 8 weeks after surgery, respectively. Antisera specific for each transporter (1:1000–10,000 dilution) were used as primary antibodies. Control, membranes obtained from normal kidney; E(−), Nx rats administered vehicle; E(+), Nx rats administered everolimus.

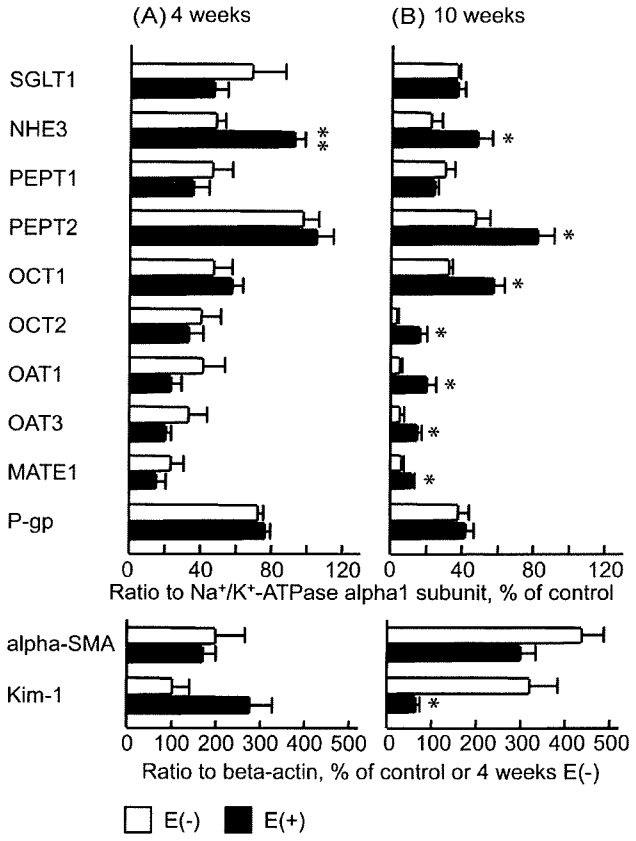

Fig. 9. Effects of everolimus on the protein expression levels of transporters, alpha-SMA and Kim-1. Four weeks (A) and 10 weeks (B) represent groups in which a 14-day subcutaneous administration of everolimus (2 mg/kg/day) or vehicle was initiated at 2 and 8 weeks after surgery, respectively. The densitometric ratio relative to control rat kidneys (for transporters and alpha-SMA) or to the group 4 weeks E(−) (for Kim-1) were shown as the reference. As internal standards, Na^+/K^+-ATPase alpha1 subunit (for transporters) and beta-actin (for alpha-SMA and Kim-1) were used. Values are the mean ± SEM. E(−), 5/6 nephrectomized rats administered vehicle; E(+), 5/6 nephrectomized rats administered everolimus. $^*P < 0.05$, $^{**}P < 0.01$, significantly different from E(−) rats.

in the proximal tubules, and this pharmacological response is at least a part accountable for the decrease in albuminuria.

We previously found that the tubular secretion of ionic drugs such as *para*-aminohippuric acid and cimetidine was markedly decreased in Nx rats, and a down-regulation of organic ion transporters was responsible for these pharmacokinetic changes [3–6]. Interestingly, everolimus recovered the protein expression of these transporters even in the advanced stage of CRF (Fig. 8). Furthermore, it was revealed that the everolimus-treatment restored the expression levels of NHE3 and PEPT2 (Fig. 8), which play roles in maintaining the pH gradient across the luminal membrane [36] and reabsorption of oligopeptides and peptide mimics [37] in the proximal tubules, respectively. In the kidney, numerous membrane transporters play crucial roles as a detoxicating mechanism in the elimination of organic compounds, such as uremic toxin, into urine via tubular secretion [9,38–40]. Therefore, mTOR inhibition by everolimus in CRF is indicated to be able to bring restoration of tubular functions including the reabsorption of albumin and nutrients, homeostasis in the acid–base balance and detoxication by recovering the membrane transporters in the polarized epithelia.

Although Kim-1 has been characterized as a urinary biomarker of acute kidney injury, little information about its role was clarified in progressive renal failure [41]. In the present study, we have first found that the expression of Kim-1 was induced in the proximal tubules with time after nephrectomy (Fig. 6). The expression of Kim-1 is increased in the injured kidney [23] and is predominantly localized to the apical membrane acting as a receptor for the phagocytosis of apoptotic cells by the proximal tubular epithelium itself [42]. In FITC-albumin-administered rat kidneys, the red signal area with Kim-1 antibody was almost independent from the area of green signals for FITC-albumin (Fig. 7G and H). As expected, the red signal area with Kim-1 antibody was decreased with the increase in the condensed green signals for FITC-albumin in response to the administration of everolimus (Figs. 6 and 7). These results suggested that the inhibition of the mTOR pathway recovered the tubular function coinciding with the amelioration of progressive tubular dysfunction and decrease the expression of Kim-1 in CRF proximal tubules.

Tubular atrophy and interstitial fibrosis are the final common steps on the progression of chronic kidney disease [1]. Epithelial-mesenchymal transition (EMT) is considered to have a crucial role in this pathogenesis [43]. In Nx rats, EMT was observed in the remnant kidney, and alpha-SMA was shown to be a marker for EMT [44,45]. On the other hand, it was reported that the activation of

the mTOR pathway regulate transforming growth factor-beta induced EMT [46] and that the inhibition of mTOR may be effective in intervention for EMT in chronic nephropathies [47]. In this study, treatment with everolimus abolished the accumulation of alpha-SMA in the tubulointerstitial space (Fig. 6). Furthermore, histological analysis revealed that the dilatation of proximal tubules was reduced by the treatment with everolimus (Fig. 5). These results suggest that the constitutively active mTOR pathway modulates dysfunction of proximal tubular epithelial cells via EMT in CRF.

In addition to improving renal tubular functions, everolimus also inhibited the accumulation of alpha-SMA (Fig. 6B and D) and infiltration of macrophages (Fig. 6F and H) without affecting the Ccr or the level of BUN (Table 1) when administration of everolimus was started at 8 weeks after Nx. These results are consistent with the report by Diekmann et al. [19] with another mTOR inhibitor, rapamycin. However, the effects of everolimus were rather complex when the administration was initiated at 2 weeks after renal ablation. Everolimus decreased Ccr and increased the level of BUN, but showed renoprotective effects as indicated by the decreased levels of alpha-SMA and ED1 (Fig. 6) and did not induce further albuminuria (Table 1). Because the hypertrophic responses are predominantly observed within 4 weeks after Nx [38], high doses of mTOR inhibitors could decrease single nephron-GFR and increased both afferent and efferent glomerular resistance without a reduction of whole kidney GFR in normal rat kidney [48]. Therefore, everolimus might cause further reductions of renal function in the rats during the vigorous compensative adaptation. However, further studies are needed to clarify the discrepancy in the pharmacological response to the inhibition of mTOR after Nx, and the limitation of mTOR inhibitors for CRF focusing on disease stage.

In summary, the constitutive activated mTOR pathway in the proximal tubules was revealed in the rat remnant kidneys. In addition, mTOR inhibitors had renoprotective effects to ameliorate progressive tubular dysfunction in the advanced stage of CRF. Although the precise molecular mechanisms of signal transduction in the progressive renal failure by which the inhibition of mTOR leads to these effects remain to be elucidated, these results suggested an additional therapeutic approach to end-stage renal disease with mTOR inhibitors focusing on the proximal tubular functions.

Acknowledgments

This work was supported in part by a grant-in-aid for Research on Biological Markers for New Drug Development, Health and Labour Sciences Research Grants from the Ministry of Health, Labour and Welfare of Japan (08062855 to S. Masuda), by the Japan Health Science Foundation "Research on Health Sciences Focusing on Drug Innovation" (KH23303 to S. Masuda), by a Grant-in-Aid for Scientific Research (A) (20249036 to K. Inui), Grant-in-Aid for Young Scientists (A) (18689016 to S. Masuda) and Grant-in-Aid for JSPS Fellows (20-2438 to K. Nishihara) from the Ministry of Education, Science, Culture, Sports and Technology of Japan (MEXT). K. Nishihara is a Research Fellow of the Japan Society for the Promotion of Science (JSPS).

References

[1] Taal MW, Brenner BM. Adaptation to nephron loss. In: Brenner BM, editor. The kidney. WB Saunders; 2008. p. 783–819.
[2] Remuzzi G, Bertani T. Pathophysiology of progressive nephropathies. N Engl J Med 1998;339:1448–56.
[3] Takeuchi A, Masuda S, Saito H, Doi T, Inui K. Role of kidney-specific organic anion transporters in the urinary excretion of methotrexate. Kidney Int 2001;60:1058–68.
[4] Ji L, Masuda S, Saito H, Inui K. Down-regulation of rat organic cation transporter rOCT2 by 5/6 nephrectomy. Kidney Int 2002;62:514–24.
[5] Horiba N, Masuda S, Takeuchi A, Saito H, Okuda M, Inui K. Gene expression variance based on random sequencing in rat remnant kidney. Kidney Int 2004;66:29–45.
[6] Nishihara K, Masuda S, Ji L, Katsura T, Inui K. Pharmacokinetic significance of luminal multidrug and toxin extrusion 1 in chronic renal failure rats. Biochem Pharmacol 2007;73:1482–90.
[7] Kwon TH, Frokiaer J, Fernandez-Llama P, Maunsbach AB, Knepper MA, Nielsen S. Altered expression of Na transporters NHE-3, NaPi-II, Na-K-ATPase, BSC-1, and TSC in CRF rat kidneys. Am J Physiol 1999;277:F257–70.
[8] Takahashi K, Masuda S, Nakamura N, Saito H, Futami T, Doi T, et al. Upregulation of H(+)-peptide cotransporter PEPT2 in rat remnant kidney. Am J Physiol Renal Physiol 2001;281:F1109–16.
[9] Sun H, Frassetto L, Benet LZ. Effects of renal failure on drug transport and metabolism. Pharmacol Ther 2006;109:1–11.
[10] Matsuzaki T, Watanabe H, Yoshitome K, Morisaki T, Hamada A, Nonoguchi H, et al. Downregulation of organic anion transporters in rat kidney under ischemia/reperfusion-induced acute renal failure. Kidney Int 2007;71:539–47.
[11] Fingar DC, Blenis J. Target of rapamycin (TOR): an integrator of nutrient and growth factor signals and coordinator of cell growth and cell cycle progression. Oncogene 2004;23:3151–71.
[12] Wullschleger S, Loewith R, Hall MN. TOR signaling in growth and metabolism. Cell 2006;124:471–84.
[13] Inoki K, Corradetti MN, Guan KL. Dysregulation of the TSC-mTOR pathway in human disease. Nat Genet 2005;37:19–24.
[14] Stallone G, Infante B, Schena A, Battaglia M, Ditonno P, Loverre A, et al. Rapamycin for treatment of chronic allograft nephropathy in renal transplant patients. J Am Soc Nephrol 2005;16:3755–62.
[15] Pontrelli P, Rossini M, Infante B, Stallone G, Schena A, Loverre A, et al. Rapamycin inhibits PAI-1 expression and reduces interstitial fibrosis and glomerulosclerosis in chronic allograft nephropathy. Transplantation 2008;85:125–34.
[16] Shillingford JM, Murcia NS, Larson CH, Low SH, Hedgepeth R, Brown N, et al. The mTOR pathway is regulated by polycystin-1, and its inhibition reverses renal cystogenesis in polycystic kidney disease. Proc Natl Acad Sci U S A 2006;103:5466–71.
[17] Nagai K, Matsubara T, Mima A, Sumi E, Kanamori H, Iehara N, et al. Gas6 induces Akt/mTOR-mediated mesangial hypertrophy in diabetic nephropathy. Kidney Int 2005;68:552–61.
[18] Lloberas N, Cruzado JM, Franquesa M, Herrero-Fresneda I, Torras J, Alperovich G, et al. Mammalian target of rapamycin pathway blockade slows progression of diabetic kidney disease in rats. J Am Soc Nephrol 2006;17:1395–404.
[19] Diekmann F, Rovira J, Carreras J, Arellano EM, Banon-Maneus E, Ramirez-Bajo MJ, et al. Mammalian target of rapamycin inhibition halts the progression of proteinuria in a rat model of reduced renal mass. J Am Soc Nephrol 2007;18:2653–60.
[20] Vogelbacher R, Wittmann S, Braun A, Daniel C, Hugo C. The mTOR inhibitor everolimus induces proteinuria and renal deterioration in the remnant kidney model in the rat. Transplantation 2007;84:1492–9.
[21] Yokomasu A, Yano I, Sato E, Masuda S, Katsura T, Inui K. Effect of intestinal and hepatic first-pass extraction on the pharmacokinetics of everolimus in rats. Drug Metab Pharmacokinet 2008;23:469–75.
[22] Masuda S, Saito H, Nonoguchi H, Tomita K. Inui K. mRNA distribution and membrane localization of the OAT-K1 organic anion transporter in rat renal tubules. FEBS Lett 1997;407:127–31.
[23] Ichimura T, Bonventre JV, Bailly V, Wei H, Hession CA, Cate RL, et al. Kidney injury molecule-1 (KIM-1), a putative epithelial cell adhesion molecule containing a novel immunoglobulin domain, is up-regulated in renal cells after injury. J Biol Chem 1998;273:4135–42.
[24] Ogihara H, Saito H, Shin BC, Terado T, Takenoshita S, Nagamachi Y, et al. Immuno-localization of H+/peptide cotransporter in rat digestive tract. Biochem Biophys Res Commun 1996;220:848–52.
[25] Takahashi K, Nakamura N, Terada T, Okano T, Futami T, Saito H, et al. Interaction of beta-lactam antibiotics with H+/peptide cotransporters in rat renal brush-border membranes. J Pharmacol Exp Ther 1998;286:1037–42.
[26] Urakami Y, Okuda M, Masuda S, Saito H, Inui K. Functional characteristics and membrane localization of rat multispecific organic cation transporters, OCT1 and OCT2, mediating tubular secretion of cationic drugs. J Pharmacol Exp Ther 1998;287:800–5.
[27] Urakami Y, Nakamura N, Takahashi K, Okuda M, Saito H, Hashimoto Y, et al. Gender differences in expression of organic cation transporter OCT2 in rat kidney. FEBS Lett 1999;461:339–42.
[28] Hashida T, Masuda S, Uemoto S, Saito H, Tanaka K, Inui K. Pharmacokinetic and prognostic significance of intestinal MDR1 expression in recipients of living-donor liver transplantation. Clin Pharmacol Ther 2001;69:308–16.
[29] Tao Y, Kim J, Schrier RW, Edelstein CL. Rapamycin markedly slows disease progression in a rat model of polycystic kidney disease. J Am Soc Nephrol 2005;16:46–51.
[30] Chen JK, Chen J, Neilson EG, Harris RC. Role of mammalian target of rapamycin signaling in compensatory renal hypertrophy. J Am Soc Nephrol 2005;16:1384–91.
[31] Andreucci M, Fuiano G, Presta P, Esposito P, Faga T, Bisesti V, et al. Radiocontrast media cause dephosphorylation of Akt and downstream signaling targets in human renal proximal tubular cells. Biochem Pharmacol 2006;72:1334–42.

[32] Mariappan MM, Shetty M, Sataranatarajan K, Choudhury GG, Kasinath BS. Glycogen synthase kinase 3beta is a novel regulator of high glucose- and high insulin-induced extracellular matrix protein synthesis in renal proximal tubular epithelial cells. J Biol Chem 2008;283:30566–75.
[33] Birn H, Christensen EI. Renal albumin absorption in physiology and pathology. Kidney Int 2006;69:440–9.
[34] Russo LM, Sandoval RM, Campos SB, Molitoris BA, Comper WD, Brown D. Impaired tubular uptake explains albuminuria in early diabetic nephropathy. J Am Soc Nephrol 2009;20:489–94.
[35] Letavernier E, Bruneval P, Vandermeersch S, Perez J, Mandet C, Belair MF, et al. Sirolimus interacts with pathways essential for podocyte integrity. Nephrol Dial Transplant 2009;24:630–8.
[36] Boron WF. Acid-base transport by the renal proximal tubule. J Am Soc Nephrol 2006;17:2368–82.
[37] Inui K, Masuda S, Saito H, Cellular. molecular aspects of drug transport in the kidney. Kidney Int 2000;58:944–58.
[38] Motohashi H, Sakurai Y, Saito H, Masuda S, Urakami Y, Goto M, et al. Gene expression levels and immunolocalization of organic ion transporters in the human kidney. J Am Soc Nephrol 2002;13:866–74.
[39] Urakami Y, Akazawa M, Saito H, Okuda M, Inui K. cDNA cloning, functional characterization, and tissue distribution of an alternatively spliced variant of organic cation transporter hOCT2 predominantly expressed in the human kidney. J Am Soc Nephrol 2002;13:1703–10.
[40] Masuda S, Terada T, Yonezawa A, Tanihara Y, Kishimoto K, Katsura T, et al. Identification and functional characterization of a new human kidney-specific H+/organic cation antiporter, kidney-specific multidrug and toxin extrusion 2. J Am Soc Nephrol 2006;17:2127–35.
[41] van Timmeren MM, Bakker SJ, Vaidya VS, Bailly V, Schuurs TA, Damman J, et al. Tubular kidney injury molecule-1 in protein-overload nephropathy. Am J Physiol Renal Physiol 2006;291:F456–64.
[42] Ichimura T, Asseldonk EJ, Humphreys BD, Gunaratnam L, Duffield JS, Bonventre JV. Kidney injury molecule-1 is a phosphatidylserine receptor that confers a phagocytic phenotype on epithelial cells. J Clin Invest 2008;118:1657–68.
[43] Kalluri R, Neilson EG. Epithelial-mesenchymal transition and its implications for fibrosis. J Clin Invest 2003;112:1776–84.
[44] Kliem V, Johnson RJ, Alpers CE, Yoshimura A, Couser WG, Koch KM, et al. Mechanisms involved in the pathogenesis of tubulointerstitial fibrosis in 5/6-nephrectomized rats. Kidney Int 1996;49:666–78.
[45] Ng YY, Huang TP, Yang WC, Chen ZP, Yang AH, Mu W, et al. Tubular epithelial-myofibroblast transdifferentiation in progressive tubulointerstitial fibrosis in 5/6 nephrectomized rats. Kidney Int 1998;54:864–76.
[46] Lamouille S, Derynck R. Cell size and invasion in TGF-beta-induced epithelial to mesenchymal transition is regulated by activation of the mTOR pathway. J Cell Biol 2007;178:437–51.
[47] Wu MJ, Wen MC, Chiu YT, Chiou YY, Shu KH, Tang MJ. Rapamycin attenuates unilateral ureteral obstruction-induced renal fibrosis. Kidney Int 2006;69:2029–36.
[48] Sabbatini M, Sansone G, Uccello F, De Nicola L, Nappi F, Andreucci VE. Acute effects of rapamycin on glomerular dynamics: a micropuncture study in the rat. Transplantation 2000;69:1946–90.

Heterozygous variants of multidrug and toxin extrusions (MATE1 and MATE2-K) have little influence on the disposition of metformin in diabetic patients

Kana Toyama[a], Atsushi Yonezawa[a], Masahiro Tsuda[a], Satohiro Masuda[a], Ikuko Yano[a], Tomohiro Terada[a], Riyo Osawa[a], Toshiya Katsura[a], Masaya Hosokawa[b], Shimpei Fujimoto[b], Nobuya Inagaki[b] and Ken-Ichi Inui[a]

Multidrug and toxin extrusions (MATE1/SLC47A1 and MATE2-K/SLC47A2) play important roles in the renal excretion of metformin. We have previously identified the nonsynonymous *MATE* variants with functional defects at low allelic frequencies. The purpose of this study was to evaluate the effects of heterozygous *MATE* variants on the disposition of metformin in mice and humans. Pharmacokinetic parameters of metformin in *Mate1*(±) heterozygous mice were comparable with those in *Mate1*(+/+) wild-type mice. Among 48 Japanese diabetic patients, seven patients carried heterozygous *MATE* variant and no patient carried homozygous *MATE* variant. There was no significant difference in oral clearance of metformin with or without heterozygous *MATE* variants. In addition, creatinine clearance, but not heterozygous *MATE* variants, significantly improved the model fit of metformin clearance by statistical analysis using the nonlinear mixed-effects modeling program. In conclusion, heterozygous *MATE* variants could not influence the disposition of metformin in diabetic patients. *Pharmacogenetics and Genomics* 20:135–138 © 2010 Wolters Kluwer Health | Lippincott Williams & Wilkins.

Pharmacogenetics and Genomics 2010, 20:135–138

Keywords: creatinine clearance, H^+/organic cation antiporter, metformin, organic cation transporter, pharmacokinetics

[a]Department of Pharmacy, Faculty of Medicine, Kyoto University Hospital and [b]Department of Diabetes and Clinical Nutrition, Graduate School of Medicine, Kyoto University, Sakyo-ku, Kyoto, Japan

Correspondence to Professor Ken-ichi Inui, PhD, Department of Pharmacy, Kyoto University Hospital, Sakyo-ku, Kyoto 606-8507, Japan
Tel: +81 75 751 3577; fax: +81 75 751 4207;
e-mail: inui@kuhp.kyoto-u.ac.jp

Received 17 September 2009 Accepted 16 November 2009

Metformin is widely used for the treatment of hyperglycemia in patients with noninsulin-dependent diabetes mellitus. The major pharmacological action of metformin involves the suppression of gluconeogenesis in the liver. Lactic acidosis is a rare but serious adverse effect of metformin, which occurs predominantly in patients with renal insufficiency. Clinical pharmacokinetic studies revealed that metformin is mainly excreted into urine in an unchanged form without hepatic metabolism, and that the renal clearance of metformin is approximately five times higher than creatinine clearance (Ccr) [1], suggesting that renal tubular secretion is a major route of metformin elimination. In human proximal tubules, multidrug and toxin extrusion 1 (MATE1/SLC47A1) and a kidney-specific isoform MATE2-K/SLC47A2 are localized at the brush-border membranes, which were characterized as H^+/organic cation antiporters [2]. In rodents, Mate1, but not Mate2, is expressed in the kidney [2]. Metformin is a substrate for MATE1 and MATE2-K, as well as organic cation transporter 2 (OCT2/SLC22A2), which is localized at the basolateral membranes of the kidney [2,3]. The functional significance of MATE in the kidney was previously shown using *Mate1* knockout mice [4]. On the basis of these backgrounds and findings, MATE1 and MATE2-K could play key roles in metformin tubular secretion in humans.

Genetic variants in *MATE* genes are likely to be one of the factors for interindividual variability in metformin pharmacokinetics and pharmacodynamics. Recently, we and another group identified nonsynonymous single nucleotide polymorphisms (SNPs) in coding region of *MATE* genes, some of which reduced the transport activity [5,6]. In addition, Becker *et al.* [7] reported that rs2289669G > A SNP in the *MATE1* gene was associated with the glucose-lowering effect, but metformin pharmacokinetics was not evaluated. Tzvetkov *et al.* [8] demonstrated that there was no relationship between the same SNP and metformin pharmacokinetics. However, rs2289669G > A SNP in the *MATE1* gene was located in noncoding intron region and there was no information about the effect of this non-coding SNP on the transport activity. Therefore, it is not clear whether the functional reduced nonsynonymous *MATE* variants alter metformin disposition. The allelic frequencies of all *MATE* variants were quite low, in the range of 0.6–2.4% [5,6]. Homozygous variants with functional loss of transport activity decrease drug elimination in most

Supplemental digital content is available for this article. Direct URL citations appear in the printed text and are provided in the HTML and PDF versions of this article on the journal's Website (*www.pharmacogeneticsandgenomics.com*).

1744-6872 © 2010 Wolters Kluwer Health | Lippincott Williams & Wilkins

DOI: 10.1097/FPC.0b013e328335639f

cases. The effect of heterozygous variants, in contrast, depends on the transporters and the drugs. In the breast cancer resistance protein (*BCRP/ABCG2*) gene, heterozygous Q141K variant caused elevated oral bioavailability of its substrate [9]. These results suggested that information about the influence of heterozygous as well as homozygous *MATE* variants on metformin pharmacokinetics is required for its safe use in clinical situations. In this study, therefore, we focused on the effect of heterozygous nonsynonymous *MATE* variants on metformin disposition in diabetic patients.

Using *Mate1*(+/+) wild-type, *Mate1*(±) heterozygous and *Mate1*(−/−) homozygous mice, we first examined the pharmacokinetics of metformin (Supplemental methods, Supplemental digital content 1 *http://links.lww.com/FPC/A82*). High plasma concentration and low urinary excretion of metformin were observed in *Mate1*(−/−) mice compared with *Mate1*(+/+) mice, whereas there was no difference between *Mate1*(±) and *Mate1*(+/+) mice (Fig. 1a and b). In addition, several pharmacokinetic parameters in *Mate1*(±) mice were comparable with those in *Mate1*(+/+) mice (Supplemental Table 1, Supplemental digital content 2 *http://links.lww.com/FPC/A83*). Mate1 protein expression levels in these three genotype mice are shown in Fig. 1c. The transport of metformin by HEK293 cells expressing mouse Mate1, mouse Oct1 or mouse Oct2 was confirmed (Supplemental Fig. 1, Supplemental digital content 3 *http://links.lww.com/FPC/A84*). Based on these results, we hypothesized that the heterozygous *MATE* variants do not influence on the metformin clearance in humans as well as in mice.

To address the species difference in *MATE* genes, pharmacokinetic evaluation was also carried out in humans. Forty-eight Japanese patients with diabetes mellitus were enrolled into this study. Blood samples were obtained at 0, 4, and 9 h after metformin administration, followed by the determination of plasma concentrations and genotype for *MATE1*, *MATE2-K*, and *OCT2* genes (Supplemental methods, Supplemental digital content 1 *http://links.lww.com/FPC/A82*). The oral clearance (CL/F) of metformin in diabetic patients was estimated by the empirical Bayesian method with the nonlinear mixed-effects modeling program NONMEM using a basic model: $CL/F=\theta 1$. Two MATE1-G64D variant carriers, two MATE1-L125F variant carriers, and one MATE1-D328A variant carrier were found in this study. In the *MATE2-K* gene, the G211V variant was found in two patients. All *MATE* variant carriers were heterozygotes and included in the *MATE*-heterozygous variant group. The plasma concentration–time profile after an oral administration of metformin in *MATE*-heterozygous variant group was similar to that in *MATE*-reference group (Supplemental Fig. 2, Supplemental digital content 4 *http://links.lww.com/FPC/A85*). Patient

Fig. 1

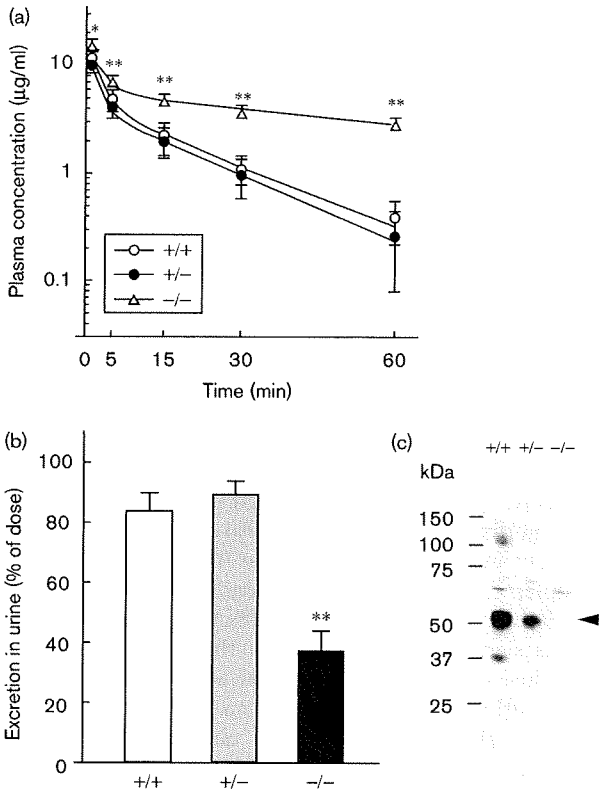

Metformin pharmacokinetic studies of *Mate1*(+/+), *Mate1*(±), and *Mate1*(−/−) mice. (a) Plasma concentration–time profiles were obtained after the intravenous administration of metformin to *Mate1* (+/+) (open circles), *Mate1*(±) (closed circles), and *Mate1*(−/−) (open triangles) mice. (b) Urinary excretion of metformin in *Mate1* (+/+) (open column), *Mate1*(±) (gray column), and *Mate1*(−/−) (closed column) mice were calculated using urine samples collected for 60 min after the drug administration. Each column represents the mean ± SD for six to eight mice. $*P<0.05$, $**P<0.01$, significantly different from *Mate1*(+/+) mice. (c) Western blot analysis of Mate1 in renal brush-border membrane fractions was carried out. The arrowhead indicates the position of mouse Mate1.

characteristics were similar between the two groups. There was no statistically significant difference in metformin CL/F between the *MATE*-heterozygous variant group and the *MATE*-reference group (Table 1). All of 11 *OCT2* variant carriers were also heterozygotes. Only one patient carried both MATE1-G64D and OCT2-A270S variants. The CL/F values of the *MATE*-variant group, the *OCT2*-variant group and both the *MATE*-variant and *OCT2*-variant group were comparable with those of the reference group (Supplemental Table 2, Supplemental digital content 5 *http://links.lww.com/FPC/A86*).

To determine the most important factor contributing to interindividual variability in metformin CL/F, we examined the relationship between CL/F and patient characteristics, such as age, sex, renal function, and

Table 1 Patient characteristics and effects of heterozygous *MATE* variants on metformin oral clearance in 48 Japanese patients with diabetes mellitus

	MATE reference	MATE-heterozygous variant[a]
Patients	41	7
Sex (male/female)	17/24	1/6
Age (years)	62±10	67±8
BMI (kg/m^2)	27±4	25±3
Metformin CL/F (ml/min)	603±137	658±115
Ccr (ml/min)	98±34	83±37
eGFR (ml/min)	71±23	71±21

Ccr, 24-h creatinine clearance; CL/F, oral clearance of metformin; eGFR, estimated glomerular filtration rate; MATE, multidrug and toxin extrusion.
[a]*MATE*-heterozygous variant includes MATE1-G64D ($n=2$), MATE1-L125F ($n=2$), MATE1-D328A ($n=1$), MATE2-K-G211V ($n=2$). No patient carried other *MATE* variants; MATE1-V10L, MATE1-A310V, MATE1-V338I, MATE1-N474S, MATE1-V480M, MATE1-C497S, MATE1-Q519H, and MATE2-K-K64N. Data are expressed as mean±SD. There was no statistically significant difference between two groups.

transporter genetic variations. Regression analysis showed that metformin CL/F was positively correlated with both Ccr and estimated glomerular filtration rate (eGFR) (Supplemental Fig. 3, Supplemental digital content 6 *http://links.lww.com/FPC/A87*). In NONMEM analysis, model fit was significantly improved for the models using the individual Ccr or eGFR compared with the basic model (CL/F=θ1). However, there was no improvement in the models with age, sex or genetic variants of the *MATE* or *OCT2* gene. A negative of twice the log likelihood difference (−2LLD) value was higher in the model using Ccr than that using eGFR (Supplemental Table 3, Supplemental digital content 7 *http://links.lww.com/FPC/A88*). The incorporation of Ccr into the basic model explained part of the interindividual variability in CL/F, with its value decreasing from 26.1 to 19.6%.

Interindividual variability in MATE activity is likely to affect the pharmacokinetics of metformin. Examination with *Mate1* knockout mice strongly suggested the pharmacokinetic alternation in humans with the functional defect homozygous variants [4]. However, homozygous variants in *MATE1* and *MATE2-K* genes were reported to be quite rare [5,6]. Therefore, we examined the pharmacokinetic significance of the heterozygous *MATE* variants to clarify whether we should pay attention to these genotypes in the clinical situations. As expected from the animal data, the heterozygous *MATE* variants did not affect the disposition of metformin in humans (Fig. 1 and Table 1). The rate-limiting step in the renal secretion of metformin is either the renal blood flow, the tubular uptake across the basolateral membranes or efflux into the lumen at the brush-border membranes. In this study, heterozygous *MATE* variants did not affect metformin clearance, although MATE1 and MATE2-K were important for metformin secretion [2,3]. Likewise, heterozygous *OCT2* variant did not affect metformin clearance in diabetic patients, even though the pharmacokinetic effect of *OCT2* variant is still controversial [3,8,10]. The renal clearance of metformin was reported to be in the range of 335–615 ml/min in humans [1], which is comparable with renal plasma flow. These results suggested that renal blood flow is a rate-limiting factor for metformin secretion. Therefore, heterozygous *MATE* variants possibly show only a minor portion in the interindividual variation of metformin pharmacokinetics in clinical situations.

For determination of the most important factor contributing to metformin disposition among age, sex, renal function, and heterozygous variations of *MATE* and *OCT2* genes, NONMEM analysis was carried out. Consistent with previous reports [1,8], we showed that Ccr is a significant predictor of metformin clearance. Although Ccr is used clinically as a marker of GFR, Ccr is known to overestimate GFR because of the creatinine tubular secretion. Previously, we showed that creatinine is a substrate for OCT2, MATE1, and MATE2-K [2]. These reports suggested that creatinine as well as metformin is excreted into the urine by tubular secretion through organic cation transport systems in addition to glomerular filtration. Comparable with these findings, metformin CL/F had a higher correlation with Ccr than with eGFR. Therefore, Ccr is the most clinical reliable indicator of metformin disposition.

In conclusion, it was shown that heterozygous *MATE* variants as well as heterozygous *OCT2* variants do not affect metformin disposition in diabetic patients. Moreover, it was revealed that Ccr is the most important factor to predict metformin disposition in the clinical use. On account of the low allelic frequency, further studies are needed with much more patients to determine the effect of homozygous *MATE* variants on metformin disposition in clinical situations.

Acknowledgements

The authors are grateful to all the medical staff of Department of Diabetes and Clinical Nutrition, Graduate School of Medicine, Kyoto University, especially to Dr Chizumi Yamada, Dr Kazuyo Fujita, Dr Akio Obara, Dr Norio Harada, Dr Kazutaka Nagai, and Dr Shiho Takahara for excellent help. This study was supported in part by a grant-in-aid for Scientific Research (KAKENHI) from the Ministry of Education, Science, Culture, and Sports of Japan. M. Tsuda is a Research Fellow of the Japan Society for the Promotion of Science.

References

1 Scheen AJ. Clinical pharmacokinetics of metformin. *Clin Pharmacokinet* 1996; **30**:359–371.
2 Terada T, Inui K. Physiological and pharmacokinetic roles of H^+/organic cation antiporters (MATE/SLC47A). *Biochem Pharmacol* 2008; **75**:1689–1696.
3 Takane H, Shikata E, Otsubo K, Higuchi S, Ieiri I. Polymorphism in human organic cation transporters and metformin action. *Pharmacogenomics* 2008; **9**:415–422.

4 Tsuda M, Terada T, Mizuno T, Katsura T, Shimakura J, Inui K. Targeted disruption of the multidrug and toxin extrusion 1 (Mate1) gene in mice reduces renal secretion of metformin. *Mol Pharmacol* 2009; **75**:1280–1286.
5 Kajiwara M, Terada T, Ogasawara K, Iwano J, Katsura T, Fukatsu A, *et al.* Identification of multidrug and toxin extrusion (MATE1 and MATE2-K) variants with complete loss of transport activity. *J Hum Genet* 2009; **54**:40–46.
6 Chen Y, Teranishi K, Li S, Yee SW, Hesselson S, Stryke D, *et al.* Genetic variants in multidrug and toxic compound extrusion-1, hMATE1, alter transport function. *Pharmacogenomics J* 2009; **9**:127–136.
7 Becker MSL, Visser LE, van Schaik RHN, Hofman A, Uitterlinden AG, Stricker BHC. Genetic variation in the multidrug and toxin extrusion 1 transporter protein influences the glucose-lowering effect of metformin in patients with diabetes: a preliminary study. *Diabetes* 2009; **58**:745–749.
8 Tzvetkov MV, Vormfelde SV, Balen D, Meineke I, Schmidt T, Sehrt D, *et al.* The effects of genetic polymorphisms in the organic cation transporters OCT1, OCT2, and OCT3 on the renal clearance of metformin. *Clin Pharmacol Ther* 2009; **86**:299–306.
9 Sparreboom A, Gelderblom H, Marsh S, Ahluwalia R, Obach R, Principe P, *et al.* Diflomotecan pharmacokinetics in relation to ABCG2 421C>A genotype. *Clin Pharmacol Ther* 2004; **76**:38–44.
10 Chen Y, Li S, Brown C, Cheatham S, Castro RA, Leabman MK, *et al.* Effect of genetic variation in the organic cation transporter 2 on the renal elimination of metformin. *Pharmacogenet Genomics* 2009; **19**:497–504.

Loss of the BMP antagonist USAG-1 ameliorates disease in a mouse model of the progressive hereditary kidney disease Alport syndrome

Mari Tanaka,[1] Misako Asada,[2] Atsuko Y. Higashi,[1] Jin Nakamura,[2] Akiko Oguchi,[2] Mayumi Tomita,[3] Sachiko Yamada,[1] Nariaki Asada,[2] Masayuki Takase,[2] Tomohiko Okuda,[4] Hiroshi Kawachi,[5] Aris N. Economides,[6] Elizabeth Robertson,[7] Satoru Takahashi,[8] Takeshi Sakurai,[9] Roel Goldschmeding,[10] Eri Muso,[11] Atsushi Fukatsu,[3] Toru Kita,[1] and Motoko Yanagita[1,2,3]

[1]Department of Cardiovascular Medicine, [2]Career-Path Promotion Unit for Young Life Scientists, [3]Department of Artificial Kidneys, and [4]COE Formation, Graduate School of Medicine, Kyoto University, Kyoto, Japan. [5]Department of Cell Biology, Institute of Nephrology, Niigata University Graduate School of Medical and Dental Sciences, Niigata, Japan. [6]Regeneron Pharmaceuticals Inc., Tarrytown, New York. [7]Wellcome Trust Center for Human Genetics, University of Oxford, Oxford, United Kingdom. [8]Laboratory Animal Resource Center, Institute of Basic Medical Sciences, University of Tsukuba, Ibaraki, Japan. [9]Department of Molecular Neuroscience and Integrative Physiology, Graduate School of Medical Science, Kanazawa University, Kanazawa, Japan. [10]Department of Pathology, University Medical Center Utrecht, Utrecht, Netherlands. [11]Division of Nephrology and Dialysis, Department of Medicine, Kitano Hospital, Osaka, Japan.

The glomerular basement membrane (GBM) is a key component of the filtering unit in the kidney. Mutations involving any of the collagen IV genes (*COL4A3*, *COL4A4*, and *COL4A5*) affect GBM assembly and cause Alport syndrome, a progressive hereditary kidney disease with no definitive therapy. Previously, we have demonstrated that the bone morphogenetic protein (BMP) antagonist uterine sensitization–associated gene-1 (USAG-1) negatively regulates the renoprotective action of BMP-7 in a mouse model of tubular injury during acute renal failure. Here, we investigated the role of USAG-1 in renal function in *Col4a3*$^{-/-}$ mice, which model Alport syndrome. Ablation of Usag1 in *Col4a3*$^{-/-}$ mice led to substantial attenuation of disease progression, normalization of GBM ultrastructure, preservation of renal function, and extension of life span. Immunohistochemical analysis revealed that USAG-1 and BMP-7 colocalized in the macula densa in the distal tubules, lying in direct contact with glomerular mesangial cells. Furthermore, in cultured mesangial cells, BMP-7 attenuated and USAG-1 enhanced the expression of MMP-12, a protease that may contribute to GBM degradation. These data suggest that the pathogenetic role of USAG-1 in *Col4a3*$^{-/-}$ mice might involve crosstalk between kidney tubules and the glomerulus and that inhibition of USAG-1 may be a promising therapeutic approach for the treatment of Alport syndrome.

Introduction

The renal glomerular basement membrane (GBM) contributes importantly to maintenance of the structural integrity of the glomerular capillaries (1, 2). Type IV collagen is the major component of the GBM, and its mutations have been linked to the genetic disorder Alport syndrome, a progressive hereditary kidney disease associated with sensorineural deafness (3). With a genetic frequency of about 1 in 5,000 people, it counts among the more prevalent of known genetic disorders (4). The disease is caused by the mutations in any one of the genes encoding the α3, α4, and α5 chains of type IV collagen (*COL4A3*, *COL4A4*, and *COL4A5*) (5–7), and a mutation affecting 1 of these chains forming the α3/α4/α5(IV) collagen network can alter or abolish the GBM expression not only of the corresponding chain but also of the other 2 chains (8). The GBM in Alport syndrome instead retains the fetal α1/α1/α2(IV) collagen network (9), which confers an increased susceptibility to proteolytic enzyme, leading to progressive destruction of the GBM with subsequent hematuria and proteinuria, glomerulosclerosis and ultimately end-stage renal disease. The current therapy is limited to dialysis and transplantation, with a higher risk of anti-GBM disease in the transplanted organs due to immune reaction against the type IV collagen chains.

Bone morphogenetic protein–7 (BMP-7) is a promising candidate to treat Alport syndrome. BMP-7 belongs to the TGF-β superfamily (10), and the kidney is the major site of BMP-7 expression during both embryogenesis and postnatal development (11). Pharmacological doses of BMP-7 can repair damaged renal tubules and preserve renal function in several models of renal diseases, including the Col4A3 knockout model of Alport syndrome (12–20). However, the exact role of endogenous BMP-7 and its mechanism of action remain unclear. In addition, the administration of recombinant BMP-7, whose target cells are widely expressed throughout the body, might also produce some undesired extrarenal effect.

The local activity of endogenous BMPs is controlled by certain classes of binding molecules that act as positive or negative regulators of BMP signaling activity (10, 21–24). BMP antagonists function through direct association with BMP, thus inhibiting the binding of BMP to its receptors and defining the boundaries of BMP activity.

The product of uterine sensitization–associated gene-1 (USAG-1) acts as a kidney-specific BMP antagonist, and USAG-1 binds to and inhibits the biological activity of BMP-7 (22, 25). USAG-1 is

Conflict of interest: The authors have declared that no conflict of interest exists.
Citation for this article: *J Clin Invest.* 2010;120(3):768–777. doi:10.1172/JCI39569.

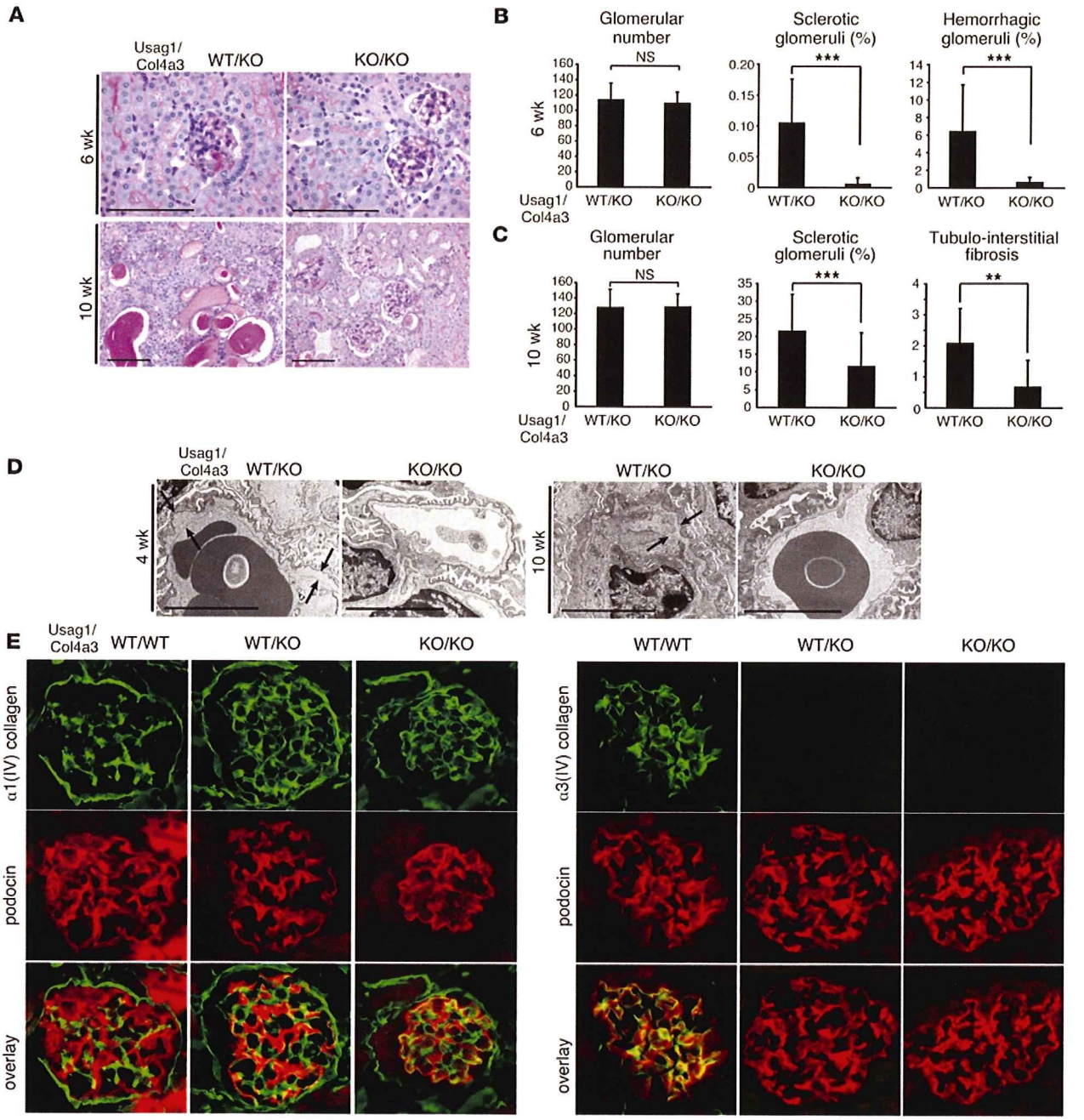

Figure 1

Usag1$^{-/-}$*Col4a3*$^{-/-}$ mice showed less glomerular and tubular injury. (**A**) Representative histological findings in *Usag1*$^{+/+}$*Col4a3*$^{-/-}$ mice (WT/KO) and *Usag1*$^{-/-}$*Col4a3*$^{-/-}$ mice (KO/KO) at 6 weeks and 10 weeks of age. Scale bars: 100 μm. (**B** and **C**) Quantitative assessment of the number of glomeruli, percentages of sclerotic and hemorrhagic glomeruli, and tubulointerstitial fibrosis score in *Usag1*$^{+/+}$*Col4a3*$^{-/-}$ mice (WT/KO) and *Usag1*$^{-/-}$*Col4a3*$^{-/-}$ mice (KO/KO) at 6 weeks (**B**, $n = 5$) and 10 weeks of age (**C**, $n = 10$). Bars indicate the mean ± SD. $^{**}P < 0.01$; $^{***}P < 0.05$. (**D**) Electron microphotographs in *Usag1*$^{+/+}$*Col4a3*$^{-/-}$ mice (WT/KO) and *Usag1*$^{-/-}$*Col4a3*$^{-/-}$ mice (KO/KO) at 4 weeks and 10 weeks of age. Arrows indicate the splitting of GBM. Scale bars: 5 μm. (**E**) Immunostaining for α1(IV) and α3(IV) collagen in the glomeruli of WT littermates (WT/WT), *Usag1*$^{+/+}$*Col4a3*$^{-/-}$ mice (WT/KO), and *Usag1*$^{-/-}$*Col4a3*$^{-/-}$ mice (KO/KO) at 6 weeks of age. Podocin was used as a podocyte marker. Note the positive staining for α1(IV) collagen along with the GBM of *Usag1*$^{+/+}$*Col4a3*$^{-/-}$ mice (WT/KO) and *Usag1*$^{-/-}$*Col4a3*$^{-/-}$ mice (KO/KO), while the staining is restricted to mesangial areas in the glomeruli of WT littermates.

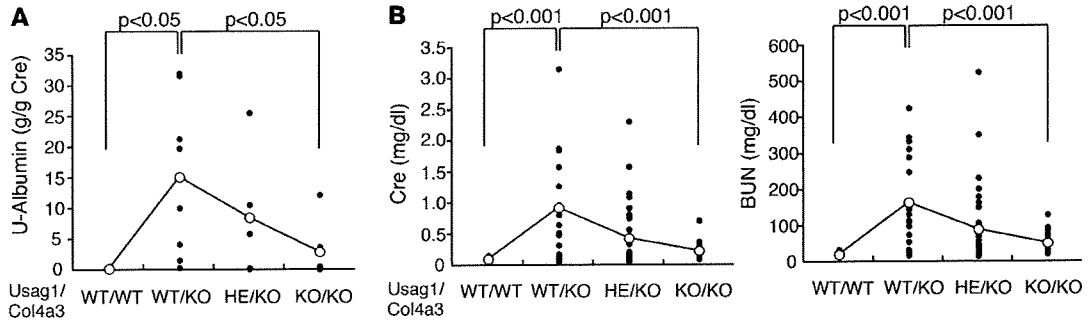

Figure 2

Usag1$^{-/-}$*Col4a3*$^{-/-}$ mice showed less albuminuria and preserved renal function. (**A**) Urinary albumin excretion normalized by urinary creatinine in WT littermates (WT/WT, $n = 4$), *Usag1*$^{+/+}$*Col4a3*$^{-/-}$ mice (WT/KO, $n = 8$), *Usag1*$^{+/-}$*Col4a3*$^{-/-}$ mice (HE/KO, $n = 5$), and *Usag1*$^{-/-}$*Col4a3*$^{-/-}$ mice (KO/KO, $n = 7$) at 6 weeks of age. Open circles represent mean value of each column, while closed circles represent individual mice. (**B**) Plasma creatinine and blood urea nitrogen (BUN) levels in WT littermates (WT/WT, $n = 20$), *Usag1*$^{+/+}$*Col4a3*$^{-/-}$ mice (WT/KO, $n = 18$), *Usag1*$^{+/-}$*Col4a3*$^{-/-}$ mice (HE/KO, $n = 34$), and *Usag1*$^{-/-}$*Col4a3*$^{-/-}$ mice (KO/KO, $n = 17$) at 10 weeks of age. Bars indicate mean ± SD. Open circles represent mean value of each column, while closed circles represent individual mice.

expressed in distal tubules and colocalizes with BMP-7 in distal convoluted tubules and connecting tubules (26). Furthermore, *Usag1*$^{-/-}$ mice are resistant to tubular injury such as acute renal failure and interstitial fibrosis, and USAG-1 is the central negative regulator of BMP function in the adult kidney (27). Because in adults the expression of USAG-1 is confined to the kidneys, targeting the activity of this protein might yield safer and more kidney-specific therapies than the administration of BMP-7 (23). For this, it will be important to first elucidate the role of USAG-1 in the pathology of progressive glomerular injury.

Here we show that genetic ablation of USAG-1 significantly attenuated the disease progression and preserved renal function in *Col4a3*$^{-/-}$ mice, a model for human Alport syndrome. The observations in this study suggest that USAG-1 might contribute to the pathogenesis of renal deterioration by a mechanism we believe to be novel that involves crosstalk between the macula densa of the distal tubules and the mesangium of the belonging glomerulus. In addition, we demonstrate that in the kidney of *Col4a3*$^{-/-}$ mice, TGF-β signaling includes phosphorylation of Smad1/5/8, transcription factors classically considered to be the downstream effectors of BMP signaling.

Results

Loss of USAG-1 slows progression of glomerular injury in Alport mice. *Col4a3*$^{-/-}$ mice, a mouse model of human Alport syndrome, develop progressive glomerulonephritis associated with tubulointerstitial fibrosis leading to renal failure. Kidneys from *Col4a3*$^{-/-}$ mice showed irregular thickening and splitting of the GBM at 4 weeks of age by electron microscopy. At 5 weeks of age, proteinuria is initiated, and at 6 weeks of age, minor glomerular lesion is occasionally observed by light microscopy. At 10 weeks of age, severe glomerular lesions associated with tubulointerstitial fibrosis are observed, and renal function deteriorates.

To test the role of USAG-1 in the progression of end-stage renal disease originating from glomerular injury, mice deficient in both *Col4a3* gene and *Usag1* gene were generated (*Usag1*$^{-/-}$*Col4a3*$^{-/-}$ mice). A histological examination of the kidneys from *Usag1*$^{+/+}$*Col4a3*$^{-/-}$ mice revealed segmental sclerosis and intraglomerular hemorrhage at 6 weeks of age, while these changes were almost completely absent in *Usag1*$^{-/-}$*Col4a3*$^{-/-}$ mice (Figure 1, A and B). At 10 weeks of age, *Usag1*$^{+/+}$*Col4a3*$^{-/-}$ mice demonstrated glomerulosclerosis associated with inflammatory cell infiltration, interstitial fibrosis, tubular atrophy, and cast formation, while these changes significantly decreased in *Usag1*$^{-/-}$*Col4a3*$^{-/-}$ mice (Figure 1, A and C).

An ultrastructural analysis of GBM using transmission electron microscopy at 4 weeks of age showed that *Usag1*$^{+/+}$*Col4a3*$^{-/-}$ mice had extensive splitting of the GBM, while *Usag1*$^{-/-}$*Col4a3*$^{-/-}$ mice showed almost normal GBM structure (Figure 1D). *Usag1*$^{-/-}$*Col4a3*$^{-/-}$ mice at 10 weeks of age also exhibited a significant preservation of GBM structure in comparison with age-matched *Usag1*$^{+/+}$*Col4a3*$^{-/-}$ mice (Figure 1D).

The immunostaining of α1(IV) or α3(IV) collagen was performed to compare the glomerular localization of α(IV) collagen in both genotypes (Figure 1E). The expression of α1(IV) collagen was detected in the GBM of both *Usag1*$^{+/+}$*Col4a3*$^{-/-}$ and *Usag1*$^{-/-}$*Col4a3*$^{-/-}$ mice, while the expression was confined to mesangial area in the WT mice. The expression of α3(IV) collagen was absent in the GBM of both *Usag1*$^{+/+}$*Col4a3*$^{-/-}$ and *Usag1*$^{-/-}$*Col4a3*$^{-/-}$ mice, while the expression was detected along the GBM in the WT mice. Therefore, regardless of the presence or absence of USAG-1, no alteration was observed in the glomerular localization of α(IV) collagen.

Usag1$^{-/-}$*Col4a3*$^{-/-}$ *mice showed less albuminuria, preserved renal function, and longer life span.* An analysis of urinary albumin excretion at 6 weeks of age is shown in Figure 2A, demonstrating significantly less albuminuria in *Usag1*$^{-/-}$*Col4a3*$^{-/-}$ mice than in *Usag1*$^{+/+}$*Col4a3*$^{-/-}$ mice. The systolic blood pressure of *Usag1*$^{-/-}$*Col4a3*$^{-/-}$ mice at 5 weeks of age was slightly lower than that of *Usag1*$^{+/+}$*Col4a3*$^{-/-}$ mice (Supplemental Figure 2; supplemental material available online with this article; doi:10.1172/JCI39569DS1). Renal function of *Usag1*$^{-/-}$*Col4a3*$^{-/-}$ mice at 10 weeks of age, as assessed by serum creatinine and blood urea nitrogen, was also significantly preserved in comparison with that of *Usag1*$^{+/+}$*Col4a3*$^{-/-}$ mice (Figure 2B), consistent with the results of renal histology and urinary albumin excretion. Furthermore, upon aging beyond 13 weeks, *Usag1*$^{-/-}$*Col4a3*$^{-/-}$ mice showed less mortality than *Usag1*$^{+/+}$*Col4a3*$^{-/-}$ mice (Supplemental Figure 1).

Inflammatory cytokine expression was significantly reduced in Usag1$^{-/-}$*Col4a3*$^{-/-}$ *mice.* As previously reported, the mRNA of inflammatory cytokines such as TNF-α, IL-1β, monocyte chemoattractant protein-1 (MCP-1), and TGF-β was upregulated in the kidneys of *Usag1*$^{+/+}$*Col4a3*$^{-/-}$ mice at 10 weeks of age (28, 29). In *Usag1*$^{-/-}$*Col4a3*$^{-/-}$ mice, however, increases in inflammatory cytokines were signifi-

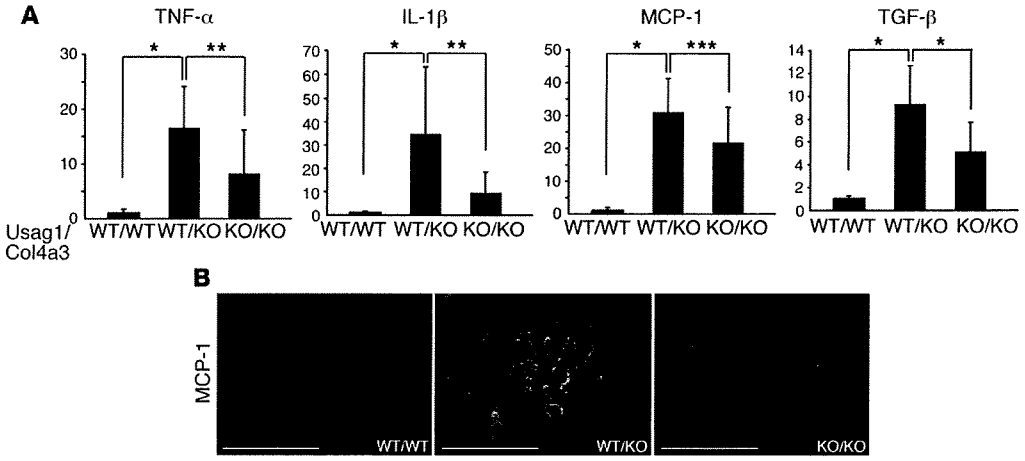

Figure 3
The expression of inflammatory cytokines significantly decreased in the kidneys of *Usag1*$^{-/-}$*Col4a3*$^{-/-}$ mice. (**A**) Real-time RT-PCR analysis of inflammatory cytokine mRNA in the kidneys of WT littermates (WT/WT), *Usag1*$^{+/+}$*Col4a3*$^{-/-}$ mice (WT/KO), and *Usag1*$^{-/-}$*Col4a3*$^{-/-}$ mice (KO/KO) at 10 weeks of age. The expression levels were normalized to those of GAPDH and expressed relative to those of WT littermates (n = 10). Bars indicate the mean ± SD. *P < 0.001; **P < 0.01; ***P < 0.05. (**B**) Representative immunostaining for MCP-1 in the kidneys of WT littermates (WT/WT), *Usag1*$^{+/+}$*Col4a3*$^{-/-}$ mice (WT/KO), and *Usag1*$^{-/-}$*Col4a3*$^{-/-}$ mice (KO/KO) at 10 weeks of age. Scale bars: 100 μm.

cantly attenuated (Figure 3A). Immunostaining for MCP-1 revealed faint expression of MCP-1 in the glomeruli of *Usag1*$^{-/-}$*Col4a3*$^{-/-}$ mice in comparison with *Usag1*$^{+/+}$*Col4a3*$^{-/-}$ mice (Figure 3B).

Enhanced Smad1/5/8 phosphorylation in Usag1$^{+/+}$*Col4a3*$^{-/-}$ *mice, but not in Usag1*$^{-/-}$*Col4a3*$^{-/-}$ *mice, was possibly activated by TGF-β signaling.* Next, the activation of Smad signaling was examined. The traditional view of the TGF-β superfamily signaling pathways assumes 2 distinct branches: a TGF-β branch that signals through Smad2/3 and a BMP branch that signals through Smad1/5/8 (30).

We observed increased phosphorylation of Smad2, the TGF-β signal transducer, in the kidneys of *Usag1*$^{+/+}$*Col4a3*$^{-/-}$ mice as compared with WT mice as well as *Usag1*$^{-/-}$*Col4a3*$^{-/-}$ mice (Figure 4A), consistent with high expression of TGF-β in *Usag1*$^{+/+}$*Col4a3*$^{-/-}$ mice (Figure 3A). The phosphorylation of Smad1/5/8, the classical BMP signal transducer, was expected to be reduced in the kidneys of *Usag1*$^{+/+}$*Col4a3*$^{-/-}$ mice due to generally low expression of BMP-7 in kidney disease models (12, 17, 26, 31). However, the phosphorylation of Smad1/5/8 was unexpectedly increased in the kidneys of *Usag1*$^{+/+}$*Col4a3*$^{-/-}$ mice in comparison with WT mice as well as *Usag1*$^{-/-}$*Col4a3*$^{-/-}$ mice.

Recently, several groups demonstrated that TGF-β activates Smad1/5 in addition to Smad2/3 in endothelial cells through novel receptor complexes (32–34). Thus, we hypothesized that the increased phosphorylation of Smad1/5/8 in the kidneys of *Usag1*$^{+/+}$*Col4a3*$^{-/-}$ mice might also have resulted from high expression of TGF-β. To test this hypothesis, we administered TGF-β to various types of cells including MDCK cells, primary mesangial cells, NRK cells (rat tubule epithelial cells), NIH3T3 cells, and HeLa cells, and demonstrated that TGF-β can activate the phosphorylation of Smad1/5/8 in addition to Smad2 in all these cell types (Figure 4B). The phosphorylation of Smad1/5/8 was induced by TGF-β at concentrations as low as 1 ng/ml (Figure 4C). Furthermore, the phosphorylation of Smad1/5/8 in the kidneys of *Usag1*$^{+/+}$*Col4a3*$^{-/-}$ mice correlated well with renal TGF-β as well as with serum creatinine levels, but not with the expression of BMP-7 (Figure 4D). Taken together, these results indicate that enhanced phosphorylation of Smad1/5/8 in *Col4a3*$^{-/-}$ mice might be due to TGF-β signaling and attenuated phosphorylation of Smad1/5/8 in *Usag1*$^{-/-}$*Col4a3*$^{-/-}$ mice might reflect reduced expression of TGF-β and disease severity.

Usag1$^{-/-}$*Col4a3*$^{-/-}$ *mice showed less expression and activity of MMPs in the kidneys.* Previous reports have demonstrated the important roles of MMPs in increasing susceptibility of defective Alport GBM to proteolytic degradation (9). The expression of *MMP* mRNA reported to be involved in this model was analyzed in the kidneys of 10-week-old mice, and this demonstrated strong upregulation of MMP-2, MMP-3, MMP-7, MMP-9, and MMP-12 in the kidneys of *Usag1*$^{+/+}$*Col4a3*$^{-/-}$ mice, while the expression of these MMPs was significantly less increased in the kidneys of *Usag1*$^{-/-}$*Col4a3*$^{-/-}$ mice (Figure 5A). The proteolytic activity of these MMPs in the kidney extracts was also determined by casein and gelatin zymography. Casein zymography showed a significant reduction in MMP-7 and MMP-12 activities (Figure 5B), and gelatin zymography demonstrated significant reduction of MMP-2 activity in the kidneys of *Usag1*$^{-/-}$*Col4a3*$^{-/-}$ mice in comparison with *Usag1*$^{+/+}$*Col4a3*$^{-/-}$ mice (Figure 5C). Also, the bands seen at 57 and 45 kDa in gelatin zymography, possibly representing MMP-3 activity (35), were significantly less in the kidneys of *Usag1*$^{-/-}$*Col4a3*$^{-/-}$ mice. Recently, it was demonstrated that expression of MMP-12 was markedly upregulated in the glomeruli of *Usag1*$^{+/+}$*Col4a3*$^{-/-}$ mice, and inhibition of MMP-12 preserved the integrity of GBM (29). Immunostaining for MMP-12 demonstrated a significant upregulation in the glomeruli and interstitium of *Usag1*$^{+/+}$*Col4a3*$^{-/-}$ mice, while the induction was attenuated in *Usag1*$^{-/-}$*Col4a3*$^{-/-}$ mice (Figure 5D). While MMP-12 is expressed by macrophages as well as glomerular cells such as podocytes (29, 36, 37), immunostaining of CD11b, a marker of monocytes and tissue macrophages, failed to demonstrate any significant infiltration of macrophages or monocytes in the glomeruli of 10-week-old *Usag1*$^{+/+}$*Col4a3*$^{-/-}$ mice (data not shown), suggesting that the glomerular MMP-12 in Alport mice was not due to the macrophages that infiltrated the glomeruli.